Ore Geology Reviews 56 (2014) 181–198

Contents lists available at ScienceDirect

Ore Geology Reviews

journal homepage: www.elsevier.com/locate/oregeorev

Geochemistry of the Huangshandong Ni–Cu deposit in northwestern China: Implications for the formation of magmatic sulfide mineralization in orogenic belts

Yu-Feng Deng [a,b], Xie-Yan Song [b,*], Lie-Meng Chen [b], Taofa Zhou [a], Franco Pirajno [a,c], Feng Yuan [a], Wei Xie [b], Dayu Zhang [a]

[a] School of Resources and Environmental Engineering, Hefei University of Technology, Hefei 230009, China
[b] State Key Laboratory of Ore Deposit Geochemistry, Institute of Geochemistry, Chinese Academy of Sciences, Guiyang 550002, China
[c] Centre for Exploration Targeting, University of Western Australia, 35, Stirling Highway, Crawley 6009; Australia

ARTICLE INFO

Article history:
Received 28 October 2012
Received in revised form 18 August 2013
Accepted 19 August 2013
Available online 23 August 2013

Keywords:
Magmatic Ni–Cu sulfide deposit
Orogenic belts
Metasomatized mantle
Huangshandong intrusion
Xinjiang

ABSTRACT

The Huangshandong Ni–Cu sulfide deposit is located at the southern margin of the Central Asian Orogenic Belt (CAOB) in north Xinjiang, NW China. The deposit contains ~135 Mt of sulfide ores grading 0.27 wt.% Cu, 0.52 wt.% Ni. The deposit is hosted by an Early Permian mafic–ultramafic complex predominantly comprising diorite, hornblende gabbro, olivine gabbro, gabbronorite, lherzolite, sulfide-bearing lherzolite and ilmenite-bearing hornblende gabbro at the base of the intrusion. These rocks exhibit enrichment of large ion lithophile elements and depleted high field strength elements relative to N-MORB, and high Th/Yb ratios, indicating that the primary magma of the Huangshandong intrusion was derived from partial melting of a metasomatized mantle source, modified by subducted slab-derived melt/fluid. Intrusive relations and geochemical signatures confirm that four pulses of magma were involved in the formation of the Huangshandong intrusion. The low Se/S ratios of the sulfide ores ($63.1–166 \times 10^{-6}$) and field observations suggest that contamination by crustal S and graphite was the key trigger mechanism for sulfide saturation. The ΣPGE contents in the Huangshandong rocks and sulfide ores range from 0.25 to 99.1 ppb, lower than those of PGE-undepleted Ni–Cu sulfide deposits. High Cu/Pd ratios ($>1.5 \times 10^5$) and low Pd content (9–151 ppb) indicate that the Huangshandong sulfides segregated from PGE-depleted magma produced by early sulfide removal at depth. Model calculations indicate that the sparsely disseminated sulfide ores in the Huangshandong deposit were produced by crystallization of the sulfide liquid. The low Pd/Ir and high Ni/Ir ratios suggest that the densely disseminated sulfides segregated from the PGE-depleted magma at lower R factor values and accumulated more MSS compared to the sparsely disseminated sulfides.

1. Introduction

Although most world-class magmatic Ni–Cu deposits have been found in intrusions associated with flood basalt volcanism and in continental rift settings (Li et al., 2005; Naldrett et al., 1995; Ryan, 2000), evidence for enhanced sulfide mineralization potential at plate margin settings has been increasing in the last decade (Maier et al., 2008; Peltonen, 1995a; Pettigrew and Hattori, 2006; Ripley, 2009; Thakurta et al., 2008; Tornos et al., 2001). These deposits are thought to have formed in orogenic belts (Maier et al., 2008; Naldrett, 2009; Song and Li, 2009) and occur in groups that are oriented along the trends of major zones of tectonic convergence (Himmelberg and Loney, 1995). Compared with the deposits associated with flood basalt volcanism and in continental rift settings, the primary magma of the ore-bearing intrusions in orogenic belts is considered to result from partial melting of metasomatized mantle modified by subducted slab-derived melt/fluid (Maier et al., 2008; Peltonen, 1995b; Song and Li, 2009; Thakurta et al., 2008; Tornos et al., 2001). However, the trigger mechanism for sulfide saturation and segregation of the magmatic Ni–Cu deposits in these orogenic belts remains unclear.

Since the 1970s, several magmatic Ni–Cu deposits associated with Permian mafic–ultramafic intrusions have been found in Xinjiang, NW China, in the southern part of the Central Asian Orogenic Belt (CAOB) (Li et al., 1989; Liu et al., 2005; Wang et al., 1987; Zhang et al., 2003, 2006, 2009). The main deposits include Kalatongke, Huangshandong, Huangshanxi and Tulaergen with a total resource of one million tonnes of Ni metal, making Xinjiang the second most important region for Ni resources in China (Liu et al., 2005; Qin et al., 2003). These deposits occur along sub-parallel translithospheric faults. Most of the sulfide

* Corresponding author. Tel.: +86 851 5895538; fax: +86 851 5891664.
E-mail address: songxieyan@vip.gyig.ac.cn (X.-Y. Song).

0169-1368/$ – see front matter © 2013 Elsevier B.V. All rights reserved.
http://dx.doi.org/10.1016/j.oregeorev.2013.08.012

bearing mafic–ultramafic complexes have been dated at 270–300 Ma and consist of dunite, lherzolite, harzburgite, websterite, gabbro and norite (Han et al., 2004, 2010; Qin et al., 2011; Su et al., 2011; Sun et al., 2006; Tang et al., 2011; Zhou et al., 2004). Previous studies have reviewed and debated the tectonic setting of these sulfide-bearing intrusions (Deng et al., 2011a,b; Pirajno et al., 2008; Qin et al., 2011; Song and Li, 2009; Song et al., 2011a; Su et al., 2012; Xiao et al., 2008; Zhang et al., 2006, 2009; Zhou et al., 2004).

The Huangshandong Ni–Cu deposit contains ~135 Mt of sulfide ore with an average grade of 0.52 wt.% Ni and 0.27 wt.% Cu and is one of the largest magmatic sulfide deposits in northern Xinjiang (Li et al., 1989; Liu et al., 2005). SHRIMP U–Pb dating of zircon from the Huangshandong intrusion yielded an age of 274 ± 3 Ma, whereas a Re–Os isochron for the Ni–Cu-bearing ores yielded an age of 282 ± 20 Ma (Han et al., 2004; Mao et al., 2002). Fluid inclusions from the Huangshandong intrusion show enrichment in H_2O, suggesting that the mantle source becomes oxidized by repeated subduction of an oceanic slab (Liu and Fei, 2006). Crustal contamination and fractionation may have been the main factors leading to S-saturation (Hu et al., 2010; Mao et al., 2002; Qian et al., 2009; Tang et al., 2012; Zhou et al., 2004). However, there are few precise geochemical data to constrain the generation and evolution of the magma, and the origin of the sulfide mineralization remains controversial. Research on the Huangshandong deposit helps in understanding the genesis of magmatic Ni–Cu deposits on the southern margin of the CAOB. In this paper, we use integrated mineralogical, petrologic, and geochemical studies to understand the nature of the mantle source and the sulfide segregation processes of the Huangshandong sulfide-bearing mafic–ultramafic intrusion.

2. Geological background

The CAOB is the largest and probably the most complex Phanerozoic orogenic belt in the world, extending more than 5000 km from west to east between the Siberian craton and North China–Tarim craton. It was formed by a nearly continuous, series of subduction–accretion processes and is composed of Precambrian continental fragments, Paleozoic island arcs and oceanic crust assemblages (Sengör et al., 1993; Windley et al., 2007; Xiao et al., 2008, 2010). Although Cu, Au and polymetallic mineral systems are common in the CAOB, Ni–Cu sulfide deposits are poorly reported other than those in north China (Fig. 1a).

The Northern Tianshan orogen is located at the southern margin of the CAOB and from north to south comprises the Harlik island arc terrane, the Bogda intra-arc basin, the Dananhu island arc terrane, the Kanggurtag intra-arc basin, and the Yamansu island arc terrane (Jahn et al., 2000; Ma et al., 1993; Qin et al., 2002; Xiao et al., 2004, 2008) (Fig. 1b). The Harlik terrane is separated from the Bogda intra-arc basin by the Balkun fault. The Kanggurtag intra-arc basin is separated from the Dananhu terrane by the Kanggurtag fault to the north and from the Yamansu terrane by the Aqikkuduk fault to the south (Fig. 1b). The Harlik arc terrane consists of Ordovician metamorphosed clastics and volcaniclastics rocks, tholeiites, andesites and minor marbles. Some researchers suggested it is a Devonian–Carboniferous island arc related to southward subduction of the Kelameili ocean (Ma et al., 1993; Zhang et al., 2004).

The Bogda intra-arc basin is composed of Carboniferous bimodal volcanic rocks, marine carbonate rocks, and epicontinental detrital rocks as well as Permian volcaniclastic rocks, conglomerate and sandstone. It has been considered to be a subduction-related rift induced by oblique subduction of the ancient Asian oceanic crust (Gu et al., 2001). The Dananhu arc terrane is composed of Ordovician–Carboniferous tholeiitic basalt, calc-alkaline andesite and pyroclastic rocks, and mainly crops out along the southern margin of the Tupan–Hami basin (Li et al., 2006a; Qin et al., 2002). The geological and geochemical features of the Devonian and Carboniferous volcanic rocks and plutons imply that they are related to subduction of an oceanic lithosphere plate (Li et al., 2006a; Song et al., 2002). There are several Early Permian mafic–ultramafic intrusions in the terrane, but Ni–Cu mineralization has not been discovered (Li et al., 2006b). The Kanggurtag intra-arc basin is in fault contact with the Dananhu island arc to the north; it contains submarine lavas, turbidites, pyroclastic rocks and andesitic tuff with tuffaceous sandstone, and was thrust over the Yamansu arc terrane (BGMX, 1993; Xiao et al., 2004). It hosts several Early Permian magmatic Ni–Cu sulfide deposits along the Kanggurtag fault, such as Tudun, Huangshandong, Huangshanxi, Xiangshan, Hulu, and Tulaergen (Fig. 1c). This is known as the Huangshan–Jing'erquan Cu–Ni ore belt, extending more than 200 km, in which some new sulfide deposits were found in recent years (Mao et al., 2008; Qin et al., 2011; San et al., 2010).

The Yamansu arc terrane is characterized by Early Carboniferous basalt and andesite, with volcaniclastic and terrigenous clastic sedimentary rocks interbedded with limestones. The geochemical patterns of the basalt and andesite confirm an island arc origin (Hou et al., 2006; Ji et al., 1999). The Early Permian granites widely exposed in the Northern Tianshan are thought to have been formed during a post-orogenic extension period (Gu et al., 2006; Jahn et al., 2000; Yuan et al., 2010; Zhou et al., 2010).

3. Petrography and mineralization of the Huangshandong intrusion

The Huangshandong mafic–ultramafic complex has a long axis of 3.5 km, a maximum width of 1.2 km, and an areal extent of about 2.8 km^2 (Fig. 2a). It intruded into carbonaceous slate, siltstone and bioclastic limestone of the Lower Carboniferous Gandun Formation. The carbonaceous slates were changed to graphite–sericite–quartz hornfels through thermal metamorphism. Marble xenoliths (2 m × 30 m) and carbonaceous slate residues are present in the hornblende gabbro (Wang et al., 1987).

The Huangshandong intrusion is a well-differentiated complex comprising, from the top downwards, diorite, hornblende gabbro, olivine gabbro, gabbronorite, lherzolite, sulfide-bearing lherzolite and ilmenite-bearing hornblende gabbro at the base (Fig. 2b). The hornblende gabbro was interpreted to comprise upper and lower zones with olivine gabbro situated in a middle zone, whereas diorite occurs along the margins of the intrusion (Li et al., 1989). The contacts between these suites are generally gradational. Gabbronorite dykes are present in the western and northwestern parts of the intrusion and contain hornblende gabbro inclusions. The lherzolite lies in the lower part of the intrusion and is seen to crosscut the hornblende gabbro and gabbronorite in drillholes (Li et al., 1989). The ilmenite-bearing hornblende gabbro at the base of the intrusion is poorly studied.

Distinct mineral assemblages and sharp contacts between the lithologic phases of the Huangshandong intrusion suggest that there were three stages of magma intrusion (Li et al., 1989). The first stage formed the main part of the intrusion, including diorite, hornblende gabbro, and olivine gabbro. The second stage formed the gabbronorite dykes. Lherzolite is the main host rock for the Cu–Ni ores and represents the last magma intrusion. The sulfide-bearing lherzolite occurs in the lowermost layer of lherzolite with gradational contacts (Fig. 2b).

Twenty orebodies have been identified in the Huangshandong intrusion, most of which occur in the central western part of the intrusion. There are four types of sulfide orebodies (Fig. 2c): (1) suspended lenses in the middle and lower parts of the ultramafic rocks; (2) at the base or margin of the ultramafic rocks and the contact between hornblende gabbro and ultramafic rocks; (3) steeply dipping lenses hosted by gabbronorite; (4) small copper-rich ore veins in hornblende gabbro (Li et al., 1989). The second type of sulfide orebodies contains the main mineralization. There are three styles of sulfide ore: massive, densely disseminated, and sparsely disseminated sulfides. The contacts between the disseminated sulfides and massive sulfides are sharp (Li et al., 1989). The dominant ore minerals are pyrrhotite, pentlandite, and chalcopyrite. Pyrrhotite and pentlandite are the major sulfides and commonly form euhedral and subhedral crystals. Some pentlandite

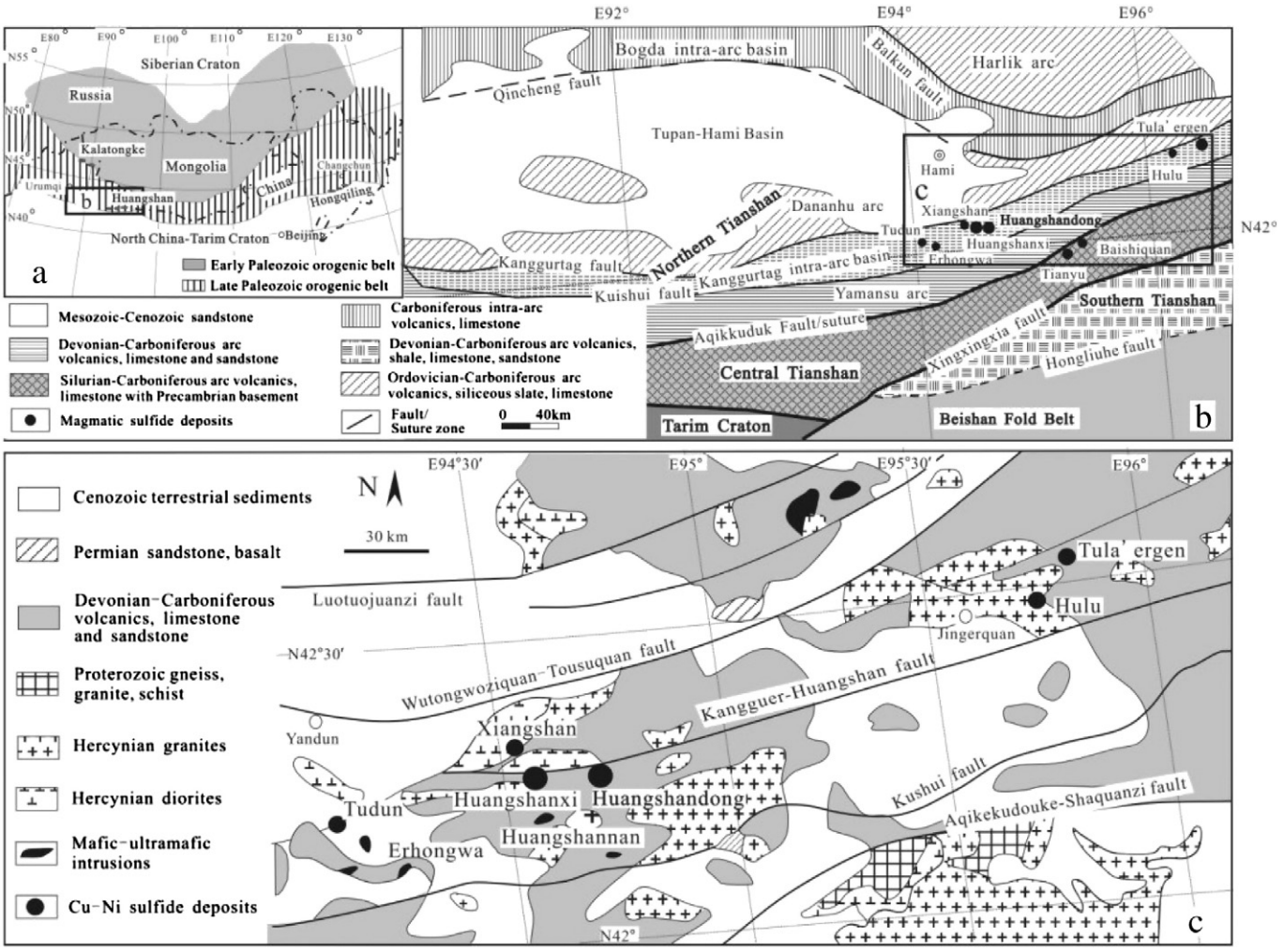

Fig. 1. (a) Schematic geological map of the Central Asian Orogenic Belt (after Hong et al., 2004); (b) simplified geological map of Northern Tianshan (after BGMX, 1993; Xiao et al., 2004); (c) simplified geological map of the Huangshan–Jingerquan copper–nickel mineralization belt (after Wang et al., 2004a,b).

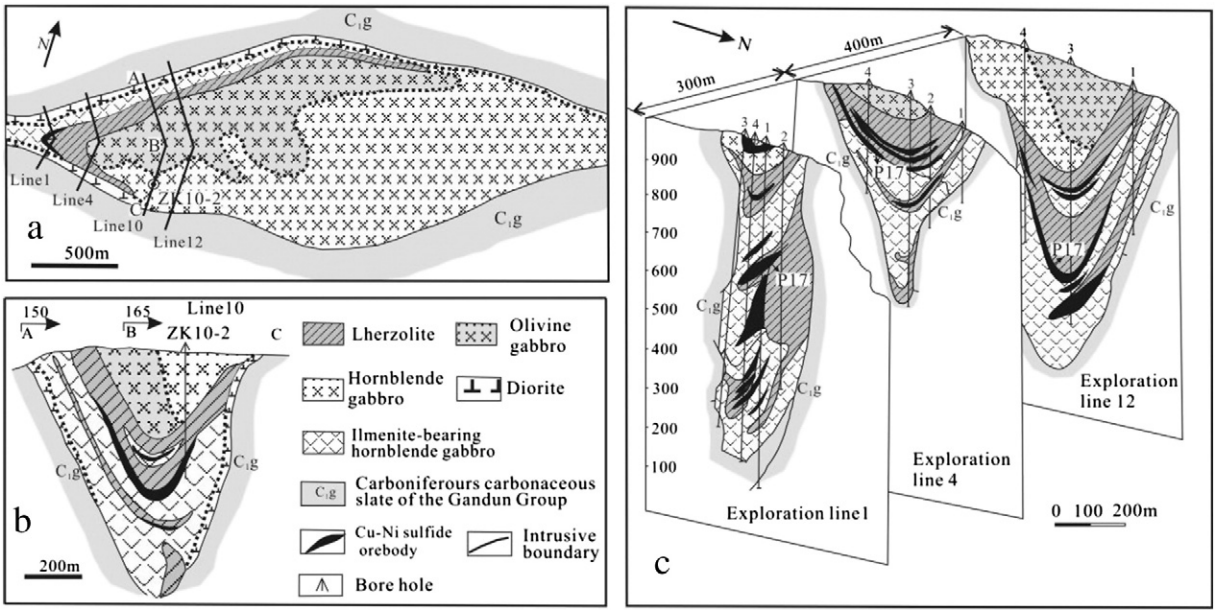

Fig. 2. Simplified geological map and cross sections of the Huangshandong intrusion, showing the distribution of lithological units and sulfide ore bodies (after Li et al., 1989).

occurs as oriented lamellae or along fractures in pyrrhotite grains (Fig. 3).

The lherzolite contains 60–65% olivine, 3–8% orthopyroxene, 2–15% clinopyroxene, 10–20% plagioclase, 5–10% hornblende, and minor phlogopite (Fig. 4a, b). The olivine crystals are sub-rounded and enclosed in large orthopyroxene, clinopyroxene, plagioclase, and hornblende. Orthopyroxene is intergrown with clinopyroxene or enclosed in clinopyroxene and hornblende. The sulfides are commonly interstitial, but small, rounded sulfide inclusions are also enclosed in some olivine crystals. Trace Cr-spinel is present as small inclusions in sulfides and silicate minerals.

The olivine gabbro contains 45–50% plagioclase, 25–30% clinopyroxene, 10–15% hornblende, 5–10% olivine, 1–5% orthopyroxene, plus minor sulfide and Fe–Ti oxides (3–8%) (Fig. 4c). Granular clinopyroxene is intergrown with plagioclase, and some has reaction coronae of hornblende. Olivine is anhedral to subhedral, and enclosed in plagioclase, clinopyroxene and hornblende. Trace orthopyroxene is enclosed in clinopyroxene. The interstitial sulfides and Fe–Ti oxides coexist with hornblende in the olivine gabbro.

The diorite contains 60–75 modal% plagioclase, 25–35% hornblende, 2–10% biotite and 2–5% quartz. The hornblende gabbro unit is composed of plagioclase (60–65%), clinopyroxene (30–35%) and hornblende (5–10%) (Fig. 4d). The clinopyroxene is intergrown with hornblende and plagioclase, and locally encloses small plagioclase crystals. By contrast, the ilmenite-bearing hornblende gabbro is composed of plagioclase (50–65%), clinopyroxene (20–40%), hornblende (5–10%), Fe–Ti oxides (2–5%) and sulfides (1–5%) plus minor orthopyroxene (1–5%) (Fig. 4e). The orthopyroxene is enclosed in hornblende and clinopyroxene. The crystallization sequence inferred from textural and mineralogical evidence is olivine → orthopyroxene → clinopyroxene + plagioclase → hornblende. Trace Cr-spinel crystallized before and during olivine crystallization. Immiscible sulfide droplets were present in the magma before or during olivine crystallization.

4. Analytical methods

Thirty-four samples used in this study are from weakly altered outcrops, underground mine workings and drill core (ZK10-2) cutting through hornblende gabbro, lherzolite, sulfide-bearing lherzolite and ilmenite-bearing hornblende gabbro to the west of the Huangshandong intrusion. Analyses of major, trace elements and platinum group elements (PGE) were conducted at the State Key Laboratory of Ore Deposit Geochemistry (SKLODG) in the Institute of Geochemistry, Chinese Academy of Science. Whole-rock abundances of major oxides were analyzed by PANalytical Axios-advance X-ray fluorescence spectrometer (XRF) on fused glass pellets with analytical uncertainties ranging from 1 to 3%. Major elements except SiO_2 and selected trace elements (Ni and Cu) in the sulfide ore were determined by inductively coupled plasma atomic emission spectroscopy (ICP-AES) at the SKLODG. SiO_2 in the sulfide ores were determined by the gravimetric method. Whole-rock S contents were measured by Leco furnace. Trace elements were determined by Inductively Coupled Plasma Mass Spectrometry (ICP-MS) using the procedure described by Qi et al. (2000). The analytical uncertainty is better than 5%.

The concentrations of PGEs were determined by a combination of NiS bead preconcentration, Te co-precipitation and ICP-MS analysis. A detailed description of the method for PGE analysis is presented by Asif and Parry (1991). Accuracy as demonstrated by analyzing reference materials, such as TDB-1 and WPR-1, is better than 10%. PGEs of the blank are generally less than 1 ppb: Ir <0.05 ppb, Ru <0.05 ppb, Rh <0.05 ppb, Pt <0.05 ppb, and Pd <0.5 ppb.

5. Results

5.1. Whole-rock major oxides

The major element compositions of the Huangshandong mafic–ultramafic rocks are listed in Table 1. In the plots and discussion that follow, all major oxide contents have been recalculated to 100% on an anhydrous and sulfide-free basis.

These samples have a wide range of SiO_2 (41.5–52.4%), MgO (5.14–36.0%), Al_2O_3 (4.54–23.2%) and TiO_2 (0.21–3.03%) contents, but have relatively low $K_2O + Na_2O$ (0.56–4.02%) contents. Comparison with the compositions of major constituent silicate minerals, the major element compositions of lherzolites are mainly controlled by the proportions of olivine, orthopyroxene and clinopyroxene in the rocks (Fig. 5a–d). The contents of major elements of hornblende gabbro, olivine gabbro and ilmenite-bearing hornblende gabbro are mainly controlled by orthopyroxene, clinopyroxene and plagioclase. Some olivine gabbro and ilmenite-bearing hornblende gabbro samples have high TiO_2 (Fig. 5e) contents due to the presence of hornblende and ilmenite and magnetite in the samples. The lower sulfide-bearing lherzolite has notably higher MgO and lower SiO_2, $Fe_2O_{3(T)}$, Al_2O_3, and $K_2O + Na_2O$ than the upper lherzolite (Figs. 5 and 6).

In plots of MgO against SiO_2, $Fe_2O_{3(T)}$, CaO, and TiO_2, hornblende gabbro, lherzolite and ilmenite-bearing hornblende gabbro exhibit discontinuous trends (Fig. 5). In contrast to hornblende gabbro, the ilmenite-bearing hornblende gabbro has higher $Fe_2O_{3(T)}$ and TiO_2, and lower SiO_2 and CaO. MgO and $Fe_2O_{3(T)}$ increase upward in the ilmenite-bearing hornblende gabbro, towards the lherzolite, whereas SiO_2 and Al_2O_3 decrease (Fig. 6).

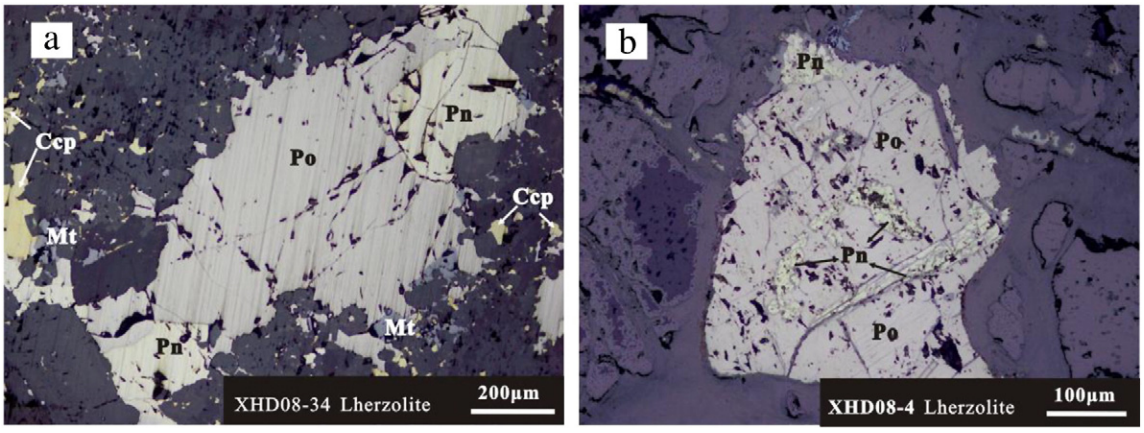

Fig. 3. Photomicrographs in reflected light showing a coexistence of pyrrhotite, pentlandite, chalcopyrite, and minor magnetite; b lamellar pentlandite along fractures in pyrrhotite grains. Ccp—chalcopyrite, Pn—pentlandite, Mt—magnetite, Po—pyrrhotite.

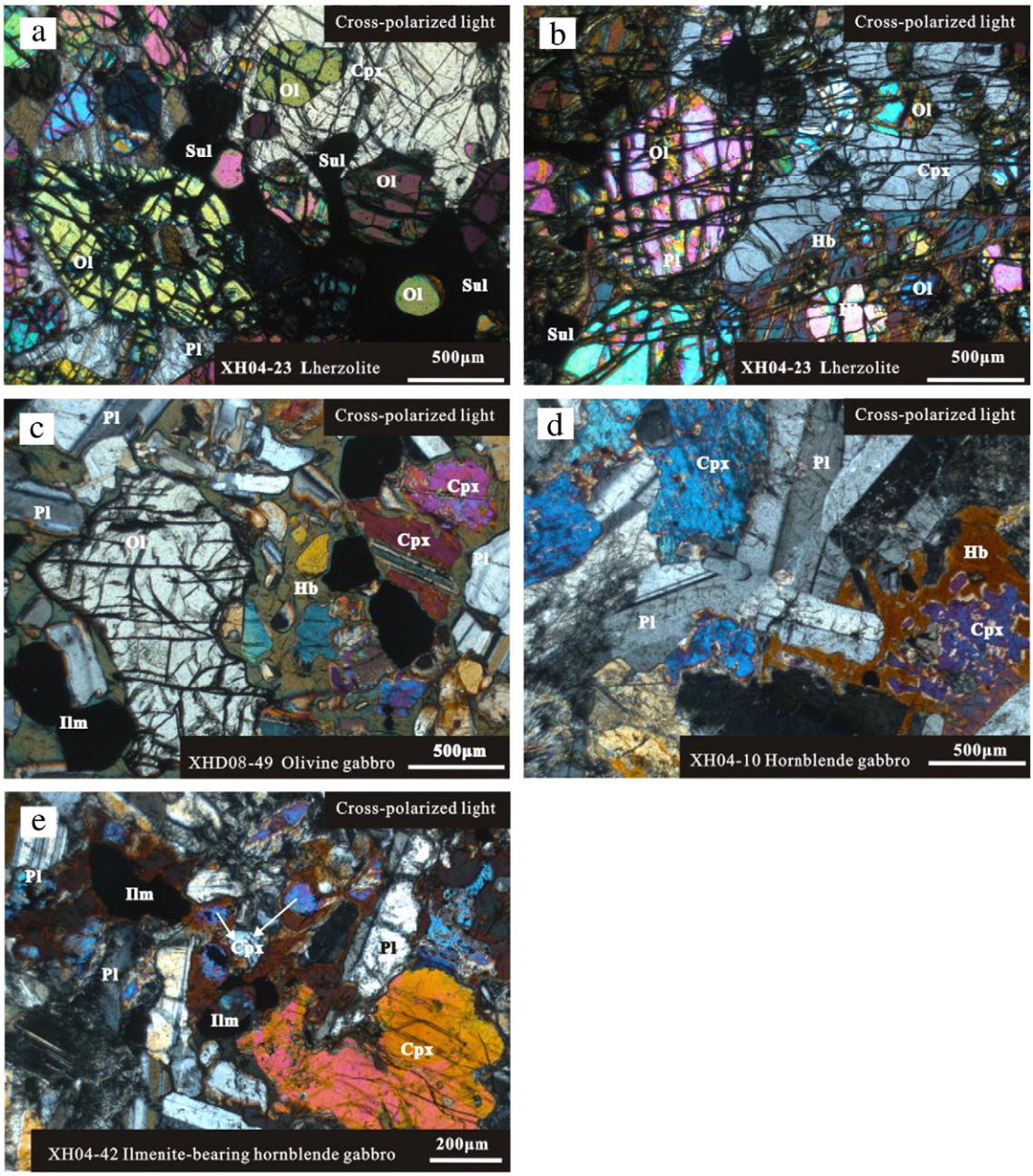

Fig. 4. Photomicrographs in cross-polarized light showing the dominant textures of lherzolite (a, b), olivine gabbro (c), hornblende gabbro (d), ilmenite-bearing hornblende gabbro with mafic minerals (e). Ol—olivine; Opx—orthopyroxene; Cpx—clinopyroxene; Pl—plagiclase; Hb—hornblende; Sul—sulfide; Ilm—ilmenite.

5.2. Trace elements

Whole-rock trace element compositions of the Huangshandong mafic–ultramafic rocks are listed in Table 1. The trace element spider diagrams normalized to normal mid-ocean ridge basalts (N-MORB) show that the Huangshandong intrusive rocks are enriched in large ion lithophile elements and depleted in heavy rare earth elements. All samples show well developed negative Nb–Ta–Ti anomalies. The lherzolite has the lowest contents of trace elements, whereas the hornblende gabbro and ilmenite-bearing hornblende gabbro contain the highest trace elements contents (Fig. 7a). The samples have variable rare earth element (REE) contents, but they are uniformly enriched in LREE relative to HREE (Fig. 7b). All samples show positive Eu anomalies because of accumulation of plagioclase. Such trace element patterns are clearly distinct from OIB, and Bachu gabbroic rocks and mafic–ultramafic dykes of the Tarim LIP (Sun and McDonough, 1989; Zhang et al., 2008; Zhou et al., 2009), and similar to those of island arc sulfide-bearing mafic intrusive rocks in the Tati and Selebi-Phikwe belts, eastern Botswana (Maier et al., 2008) (Fig. 7).

5.3. Chalcophile elements

The concentrations of PGE, Cu, Ni, S, and Se in the mafic–ultramafic rocks and sulfide ores are listed in Table 2. As shown in Fig. 8, Ni, Cu and PGE contents increase with the drilling depth; the S content in the sulfide-bearing lherzolite also increases with drilling depth. The Ni, Cu and PGE concentrations significantly increase from hornblende gabbro, lherzolite to sulfide-bearing lherzolite. Such features indicate that these

Table 1
Major oxides and trace element abundances of the Huangshandong intrusion.

Location	ZK10-2								
Rock	Hornblende gabbro			Sulfide-bearing lherzolite					
Depth (m)	135	150	165	270	285	290	295	300	303
Sample	XH04-9	XH04-10	XH04-11	XH04-18	XH04-19	XH04-20	XH04-21	XH04-22	XH04-23
Major oxides (wt.%)									
SiO_2	48.6	48.3	48.7	38.1	39.0	39.1	39.3	38.8	36.6
TiO_2	0.44	0.34	0.31	0.27	0.31	0.28	0.27	0.20	0.20
Al_2O_3	16.8	20.9	20.4	4.09	4.59	4.92	4.76	4.93	4.23
$(Fe_2O_3)_T$	6.51	5.10	5.32	15.0	13.5	13.9	14.3	13.5	17.9
MnO	0.10	0.075	0.076	0.18	0.18	0.18	0.18	0.17	0.18
MgO	10.1	7.63	8.14	32.1	33.3	32.5	32.5	31.3	30.9
CaO	11.2	11.1	11.4	2.46	2.61	2.73	2.84	2.87	2.28
Na_2O	2.40	2.87	2.42	0.39	0.48	0.52	0.50	0.41	0.40
K_2O	0.16	0.12	0.18	0.14	0.12	0.11	0.090	0.11	0.080
P_2O_5	0.045	0.042	0.037	0.061	0.034	0.038	0.043	0.059	0.036
LOI	2.70	3.51	2.95	4.60	3.68	3.93	3.55	5.22	4.94
Total	99.0	99.9	99.9	97.6	98.1	98.5	98.5	97.7	98.0
Trace elements (ppm)									
Sc	28.1	23.7	24.1	18.2	20.3	20.3	19.6	17.6	16.7
Cr	177	737	824	1571	1737	1609	1625	1548	1550
Co	18.3	48.2	52.8	155	144	135	147	137	231
Ni	27.6	93.5	110	1677	1019	1052	1602	1337	4457
Cu	5.5	29.3	25.7	390	158	179	317	256	1431
Rb	1.67	0.90	3.00	2.92	2.43	2.05	1.38	1.91	1.17
Sr	294	437	397	80	111	107	103	105	94.3
Y	9.40	7.22	6.29	5.10	5.45	4.64	4.67	3.40	3.24
Zr	12.3	20.2	17.1	26.5	22.3	19.8	16.8	18.5	14.5
Nb	0.044	0.46	0.36	0.55	0.49	0.44	0.42	0.34	0.32
Ba	29.7	28.8	29.7	23.9	26.2	21.1	19.1	17.9	15.0
La	1.92	1.74	1.46	1.82	1.25	1.20	1.24	1.35	1.03
Ce	5.05	4.21	3.70	4.50	3.53	3.16	3.27	3.39	2.55
Pr	0.77	0.62	0.54	0.60	0.50	0.44	0.47	0.45	0.34
Nd	4.22	3.46	3.10	2.69	2.83	2.32	2.38	2.07	2.91
Sm	1.24	0.99	0.90	0.69	0.75	0.66	0.63	0.50	0.44
Eu	0.57	0.74	0.58	0.24	0.29	0.25	0.25	0.22	0.21
Gd	1.37	1.14	1.03	0.81	0.76	0.65	0.71	0.51	0.45
Tb	0.27	0.22	0.20	0.15	0.15	0.13	0.13	0.083	0.093
Dy	1.56	1.20	1.16	0.83	0.95	0.77	0.83	0.53	0.53
Ho	0.31	0.23	0.25	0.18	0.17	0.17	0.17	0.11	0.11
Er	0.99	0.74	0.69	0.56	0.53	0.49	0.51	0.36	0.33
Tm	0.13	0.091	0.093	0.077	0.083	0.069	0.073	0.053	0.050
Yb	0.85	0.66	0.58	0.46	0.48	0.47	0.51	0.35	0.33
Lu	0.13	0.097	0.082	0.077	0.074	0.074	0.060	0.057	0.057
Hf	0.27	0.51	0.45	0.64	0.52	0.48	0.44	0.41	0.35
Ta	0.009	0.037	0.033	0.047	0.045	0.033	0.035	0.036	0.024
Th	0.24	0.19	0.15	0.28	0.18	0.18	0.16	0.20	0.16
U	0.033	0.083	0.058	0.10	0.073	0.062	0.054	0.088	0.052
Pb	0.58	1.12	1.50	1.93	2.67	2.01	2.03	2.34	3.91

Location	ZK10-2									
Rock	Sulfide-bearing lherzolite				Ilmenite-bearing hornblende gabbro					
Depth (m)	305	310	315	320	348	351	356	370	385	400
Sample	XH04-24	XH04-25	XH04-26	XH04-27	XH04-40	XH04-41	XH04-42	XH04-43	XH04-44	XH04-45
Major oxides (wt.%)										
SiO_2	36.5	36.6	37.2	36.1	42.6	45.4	44.9	46.1	45.7	45.9
TiO_2	0.23	0.21	0.18	0.22	0.63	0.69	1.96	2.10	2.46	2.41
Al_2O_3	4.23	4.51	4.85	4.81	15.3	17.4	18.2	22.7	21.4	22.2
$(Fe_2O_3)_T$	18.0	17.8	16.6	17.5	10.2	8.78	8.66	7.09	8.30	7.47
MnO	0.17	0.18	0.18	0.17	0.13	0.12	0.12	0.079	0.088	0.078
MgO	30.9	30.5	30.2	31.3	12.2	10.1	9.80	5.61	6.25	5.62
CaO	2.31	2.49	2.63	2.54	6.08	8.99	11.2	10.1	9.59	9.09
Na_2O	0.40	0.44	0.41	0.49	3.53	3.09	1.90	3.19	2.95	2.61
K_2O	0.080	0.090	0.080	0.080	0.12	0.12	0.13	0.16	0.23	0.18
P_2O_5	0.028	0.030	0.033	0.033	0.034	0.061	0.020	0.024	0.029	0.029
LOI	5.72	4.61	5.04	4.19	5.98	3.82	2.63	3.01	2.45	4.82
Total	98.8	97.8	97.6	97.6	96.8	98.5	99.5	100	99.4	100
Trace elements (ppm)										
Sc	16.4	10.5	15.0	7.3	11.6	22.2	25.6	21.6	31.2	25.6
Cr	1558	1265	1476	1368	150	150	141	36.1	810	37.4
Co	250	223	211	210	60.2	57.6	51.0	36.3	38.1	27.0
Ni	5102	5630	3459	4669	621	351	218	36.5	249	30.2

Table 1 (*continued*)

Location	ZK10-2									
Rock	Sulfide-bearing lherzolite				Ilmenite-bearing hornblende gabbro					
Depth (m)	305	310	315	320	348	351	356	370	385	400
Sample	XH04-24	XH04-25	XH04-26	XH04-27	XH04-40	XH04-41	XH04-42	XH04-43	XH04-44	XH04-45
Trace elements (ppm)										
Cu	1512	2970	1559	966	156	108	64.4	34.8	40.3	27.7
Rb	1.05	1.22	1.25	1.15	2.95	1.34	1.79	2.00	2.77	2.30
Sr	93.9	100	109	113	375	486	463	674	635	613
Y	3.75	3.57	3.04	3.32	4.66	11.5	6.78	5.37	13.1	8.66
Zr	13.0	15.2	14.1	13.4	19.1	39.8	13.1	10.9	18.8	18.1
Nb	0.33	0.34	0.29	0.33	0.85	0.68	0.70	0.96	1.88	1.23
Ba	15.1	16.4	16.5	19.2	47.2	56.3	35.3	64.2	71.6	67.4
La	0.81	0.91	0.89	0.90	2.02	2.37	1.17	1.49	2.12	2.10
Ce	2.29	2.45	2.22	2.32	4.22	6.26	2.66	3.17	5.31	4.28
Pr	0.32	0.34	0.31	0.36	0.59	0.97	0.46	0.46	0.93	0.72
Nd	1.76	1.79	1.70	1.78	2.90	5.76	2.65	2.54	5.46	3.60
Sm	0.45	0.47	0.41	0.47	0.62	1.73	0.82	0.83	1.88	1.11
Eu	0.19	0.22	0.21	0.23	0.45	0.81	0.64	0.73	0.10	0.74
Gd	0.51	0.49	0.44	0.52	0.68	1.76	0.97	0.90	2.01	1.23
Tb	0.096	0.10	0.081	0.096	0.14	0.35	0.21	0.16	0.41	0.27
Dy	0.58	0.64	0.59	0.61	0.80	2.18	1.31	1.07	2.53	1.70
Ho	0.13	0.12	0.11	0.12	0.17	0.43	0.25	0.21	0.48	0.33
Er	0.37	0.35	0.31	0.39	0.47	1.28	0.71	0.56	1.40	0.85
Tm	0.059	0.051	0.045	0.055	0.063	0.17	0.094	0.079	0.15	0.11
Yb	0.36	0.37	0.32	0.34	0.51	1.04	0.59	0.42	0.99	0.63
Lu	0.054	0.058	0.046	0.050	0.074	0.15	0.081	0.064	0.15	0.10
Hf	0.37	0.41	0.34	0.40	0.52	1.19	0.51	0.43	0.78	0.67
Ta	0.025	0.026	0.023	0.031	0.070	0.058	0.090	0.091	0.13	0.14
Th	0.12	0.13	0.12	0.11	0.34	0.25	0.10	0.12	0.18	0.19
U	0.036	0.050	0.047	0.050	0.11	0.084	0.040	0.034	0.054	0.056
Pb	4.35	5.57	5.48	8.33	2.26	1.55	1.16	1.27	1.60	1.84

Location	Surface samples							
Rock	Olivine gabbro							
Sample	XHD08-40	XHD08-44	XHD08-45	XHD08-46	XHD08-47	XHD08-48	XHD08-50	XHD08-51
Major oxides (wt.%)								
SiO_2	48.2	48.6	47.6	50.3	50.5	49.2	50.4	44.9
TiO_2	1.16	0.40	0.32	0.61	0.56	0.89	0.83	3.02
Al_2O_3	17.6	19.1	21.3	12.4	13.4	13.2	16.6	20.7
$(Fe_2O_3)_T$	8.69	6.26	6.57	8.54	8.06	8.79	7.77	9.04
MnO	0.14	0.10	0.071	0.16	0.16	0.17	0.14	0.10
MgO	8.19	10.4	6.89	14.3	13.5	13.2	9.99	7.80
CaO	9.00	12.8	11.9	8.48	8.42	9.13	9.79	11.9
Na_2O	2.12	1.81	0.92	1.43	1.48	1.50	2.39	1.93
K_2O	0.11	0.13	0.27	0.37	0.41	0.35	0.21	0.11
P_2O_5	0.050	0.064	0.040	0.074	0.072	0.067	0.072	0.035
LOI	4.44	0.54	2.87	2.65	3.20	2.79	1.65	
Total	99.7	100	98.8	99.3	99.7	99.3	99.9	99.5
Trace elements (ppm)								
Sc	33.9	26.3	14.3	29.7	29.7	32.8	29.8	43.9
Cr	219	543	151	468	453	427	417	24.0
Co	27.3	41.3	76.5	43.5	39.6	43.4	37.7	46.4
Ni	81.6	48.4	1302	30.9	26.0	28.0	24.9	19.2
Cu	11.6	10.3	752	5.77	3.14	11.1	8.7	23.6
Rb	0.73	2.23	6.33	9.54	11.2	7.59	2.93	1.17
Sr	476	391	547	227	237	277	394	518
Y	17.8	8.53	6.73	11.2	10.9	13.3	12.7	7.90
Zr	31.6	36.5	31.7	40.3	47.1	48.9	42.8	24.2
Nb	1.52	0.58	0.63	1.10	1.14	1.36	1.29	1.29
Ba	42.7	37.7	108	71.7	91.0	83.4	99.9	53.3
La	2.61	1.94	2.42	3.44	3.57	3.52	3.90	1.62
Ce	7.40	5.00	5.22	8.10	8.21	8.51	9.37	3.77
Pr	1.35	0.75	0.75	1.16	1.19	1.34	1.38	0.64
Nd	7.24	3.86	3.39	5.36	5.51	6.47	6.75	3.63
Sm	2.50	1.23	0.94	1.61	1.50	1.97	1.89	1.28
Eu	1.15	0.66	0.61	0.58	0.53	0.70	0.77	0.81
Gd	2.68	1.26	0.96	1.58	1.49	1.90	1.84	1.53
Tb	0.54	0.24	0.20	0.33	0.31	0.41	0.38	0.29
Dy	3.25	1.59	1.13	2.03	1.91	2.45	2.34	2.03
Ho	0.73	0.34	0.27	0.47	0.43	0.53	0.53	0.42
Er	1.86	0.93	0.73	1.26	1.24	1.47	1.38	1.02
Tm	0.27	0.13	0.10	0.18	0.18	0.21	0.20	0.13
Yb	1.58	0.79	0.64	1.14	1.14	1.36	1.22	0.86

(*continued on next page*)

Table 1 (*continued*)

Location	Surface samples							
Rock	Olivine gabbro							
Sample	XHD08-40	XHD08-44	XHD08-45	XHD08-46	XHD08-47	XHD08-48	XHD08-50	XHD08-51
Trace elements (ppm)								
Lu	0.22	0.12	0.093	0.17	0.17	0.19	0.18	0.11
Hf	1.11	0.91	0.89	1.20	1.30	1.35	1.23	0.89
Ta	0.10	0.045	0.051	0.087	0.10	0.12	0.098	0.17
Th	0.13	0.23	0.32	0.63	0.72	0.64	0.58	0.18
U	0.57	0.14	0.12	0.27	0.30	0.25	0.24	0.077
Pb	1.05	0.62	8.55	2.28	1.58	1.57	2.20	0.60

Note. LOI = loss on ignition; $(Fe_2O_3)_T$ as total Fe.

metals are concentrated at the base of the lherzolite and controlled by the content of sulfide, which is consistent with the positive correlation between Cu, Ni and S (Fig. 9). The Cu and S contents in two samples do not follow the positive correlation trend, possibly due to hydrothermal alteration.

The content of ΣPGE in the Huangshandong mafic–ultramafic rocks and sulfide ores ranges from 0.25 to 99.1 ppb. The lherzolite has higher PGE concentrations than the hornblende gabbro as shown by the primitive mantle-normalized diagrams (Fig. 10). Sulfide contents in the sulfide-mineralized samples were calculated using a procedure given in a review by Barnes and Lightfoot (2005). The mantle-normalized patterns of Cu, Ni, and PGE in recalculated 100% sulfide in the samples are illustrated in Fig. 11. Compared with two well-known Cu–Ni deposits, the PGE tenors of the Huangshandong deposit are extremely low: ~3 orders of magnitude lower than the Noril'sk–Talnakh Cu–Ni–PGE deposit and slightly lower than the Kalatongke PGE-depleted Ni–Cu deposit (Fig. 11a). In addition, the PGE contents of the Huangshandong ores are similar to those of the Selebi-Phikwe belt ores and lower than those of the Tati ores of eastern Botswana (Fig. 11b). On the Pd/Ir vs Ni/Cu diagram, most samples plot in the field of high-Mg basalts and layered intrusions (Fig. 12).

6. Discussion

6.1. Nature of the mantle source

Several studies have indicated that the magmas generated from the metasomatized mantle sources in a subduction environment are normally enriched in large ion lithophile elements (LILE) and depleted in high field strength elements (Hawkesworth et al., 1977; Johnson and Plank, 1999; Pearce, 1983; Pearce and Peate, 1995). The samples from the Huangshandong intrusion are characterized by enrichment of Rb, Ba, U, and Sr, and depletion of Nb, Ta, and Ti relative to N-MORB. On the other hand, the high positive $\varepsilon_{Nd(t)}$ values (+6.7 to +9.3) and low $(^{86}Sr/^{87}Sr)_i$ ratios (0.7025 to 0.7053) of the Huangshandong intrusion suggest that the mantle-derived magma has undergone little interaction with older continental crust (Deng et al., 2011a; Zhou et al., 2004). Thus, the favored interpretation is that the geochemical signatures of the Huangshandong intrusion resulted from partial melting of a metasomatized mantle modified by subducted slab-derived melt/fluid.

The mafic rocks of oceanic island arcs and active continental margins commonly have higher Th/Yb and lower Ta/Yb due to magma generation from the metasomatized mantle wedge above the subducted slab. As shown in Fig. 13, the Huangshandong intrusive rocks plot in the field of oceanic island arcs, similar to the samples from the Tati and Selebi-Phikwe belt of eastern Botswana, which are related to island arc mafic intrusions (Maier et al., 2008). In the Th–Hf–Ta diagram, the Huangshandong rocks have trace element compositions similar to island arc basalts, also indicating a subduction environment. The olivine- and plagioclase-hosted fluid inclusions from the Huangshandong intrusion are enriched in H_2O suggesting that the mantle source became oxidized by subduction of an oceanic slab (Liu and Fei, 2006). Experiments have indicated that the presence of H_2O can lower solidus temperatures of peridotite or lherzolite and trigger melting (Wyllie, 1982). Thus, a metasomatized mantle source modified by subducted slab-derived melt/fluid for the Huangshandong intrusion seems most likely. This is consistent with previous studies that indicated extensive subduction-related accretionary orogenesis of the Northern Tianshan during the Late Paleozoic (Chen et al., 2005, 2013; Han et al., 2006; Su et al., 2012; Windley et al., 2007; Xiao et al., 2004, 2008).

Compared to the mafic–ultramafic intrusive rocks of the Permian Tarim large igneous province, the Huangshandong intrusion is characterized by lower contents of incompatible elements, higher $\varepsilon_{Nd\ (t)}$ and more depleted Nb and Ta (Fig 7) (Deng et al., 2011a; Zhang et al., 2008; Zhou et al., 2009). These compositional differences are also highlighted in trace element diagrams (Fig. 13). Thus, geochemical data rule against a genetic link between the Huangshandong complex and the Tarim LIP magmatism.

Though the geochemical characteristics of the Huangshandong intrusive rocks are similar to those of island arc basalts, it does not mean the primary magma was necessarily generated by subduction processes. The Alaskan type intrusions formed in subduction zones are generally described as having a core of dunite surrounded by successive concentric rims of wehrlite, olivine clinopyroxenite, and hornblendite. Pyroxenes are almost exclusively clinopyroxenes and orthopyroxene occurs in very low abundance in the Alaskan type complexes (Himmelberg and Loney, 1995; Taylor, 1967). However, the Huangshandong intrusion does not show this concentric zoning, and orthopyroxene abundance is up to 25%, indicating that it is not an Alaskan type intrusion. On the other hand, the island arc related granitoid plutons (316–334 Ma), volcanic rocks (300–334 Ma) and the A-type granitoid plutons (284–288 Ma) were formed in a post-collisional environment in the Northern Tianshan (Chen et al., 2005; Hou et al., 2006; Jahn et al., 2000; Li et al., 2004, 2006c; Yuan et al., 2010), indicating that subduction ended in the Early Permian. New stratigraphic data and field mapping suggest that extensional tectonics were dominant in the Early Permian in the Turpan–Hami area and adjacent regions (Wartes and Carroll, 2002; Zhou et al., 2006). The Huangshandong intrusion was emplaced in the Early Permian, indicating that it formed in a syn-or post-collisional extensional environment. A number of studies have shown that magmas formed in post-collisional extensional environments also have geochemical characteristics similar to island arc or active continental margin magmatic rocks (Aldanmaz et al., 2000; Cesare et al., 2002; Cottin et al., 1998; Djafer et al., 2003; Song and Li, 2009; Wang et al., 2004a, b). In the Early Permian when the Northern Tianshan Ocean closed and subduction ceased (Qin et al., 2002; Zhou et al., 2004; Gu et al., 2006; Song and Li, 2009; Pirajno, 2010), a slab window formed as a result of slab break-off and led to asthenosphere upwelling (Begg et al., 2010; Song et al., 2011a,b; Li et al., 2012). The primary magma of the Huangshandong intrusion resulted from an interaction between upwelling depleted asthenospheric melts and metasomatized mantle modified by previous subduction.

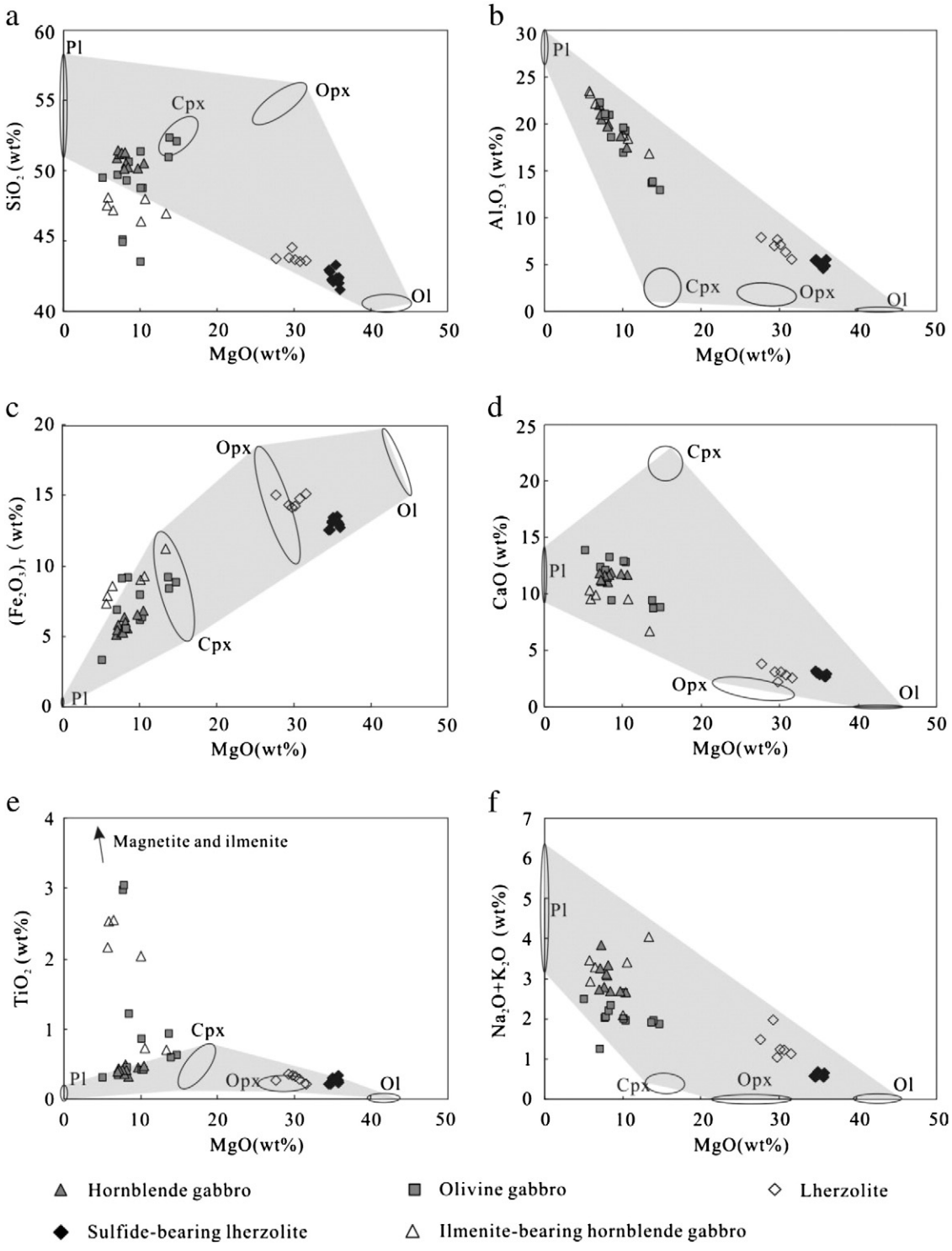

Fig. 5. Harker diagrams of the Huangshandong intrusion. Some whole-rock data of the Huangshandong intrusion are taken from Deng et al. (2011a). Ol—olivine; Opx—orthopyroxene; Cpx—clinopyroxene; Pl—plagiclase.

6.2. Magma crystallization and emplacement

Though three stages of magma intrusion have been identified (Li et al., 1989), the ilmenite-bearing hornblende gabbro at the base of the intrusion is poorly studied. The petrography and geochemistry of the hornblende gabbro are obviously different from those of the ilmenite-bearing hornblende gabbro. SiO_2, $Fe_2O_{3(T)}$, CaO, and MgO contents in the ilmenite-bearing hornblende gabbro are between those of hornblende gabbro and lherzolite. As the lherzolite is approached, MgO and $Fe_2O_{3(T)}$ of the ilmenite-bearing hornblende gabbro increase, but SiO_2 and Al_2O_3 decrease (Fig. 6). These geochemical features suggest that the ilmenite-bearing hornblende gabbro became enriched in MgO and FeO and depleted in SiO_2 and Al_2O_3 due to assimilation of mafic minerals of the lherzolite. On the other hand, if the

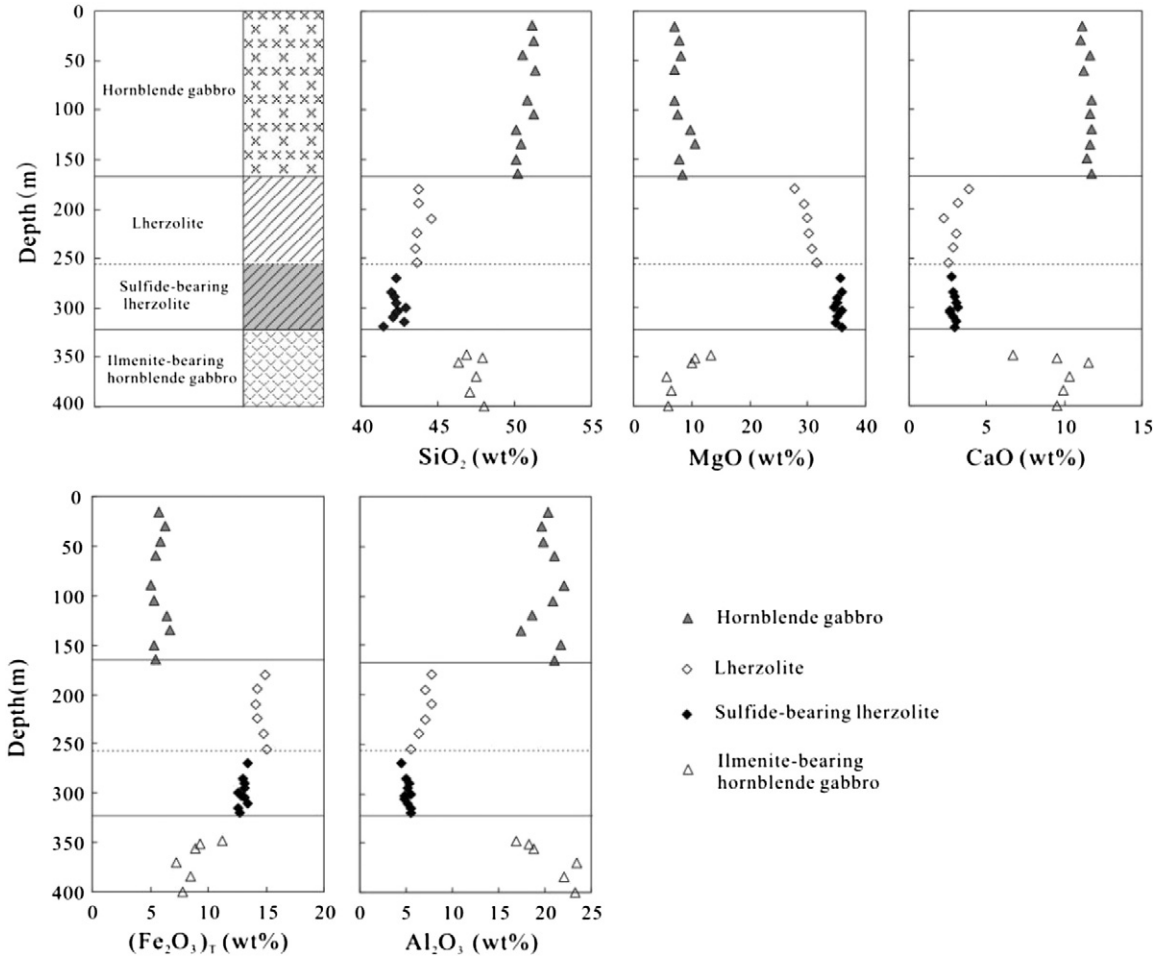

Fig. 6. Chemostratigraphic columns of SiO_2, MgO, CaO, $Fe_2O_{3(T)}$, and Al_2O_3 down drill hole ZK10-2 though the Huangshandong intrusion, showing sharp chemical variations between the upper hornblende gabbro and underlying lherzolite, and the hornblende gabbro and ilmenite-bearing hornblende gabbro. Some whole-rock data for the Huangshandong intrusion are from Deng et al. (2011a).

sulfide-bearing lherzolite intruded after emplacement of the ilmenite-bearing hornblende gabbro, MgO and $Fe_2O_{3(T)}$ and the content of mafic minerals would decrease closer to the ilmenite-bearing hornblende gabbro, which is not consistent with what is observed. Thus the evidence suggests that the ilmenite-bearing hornblende gabbro was emplaced after the lherzolite.

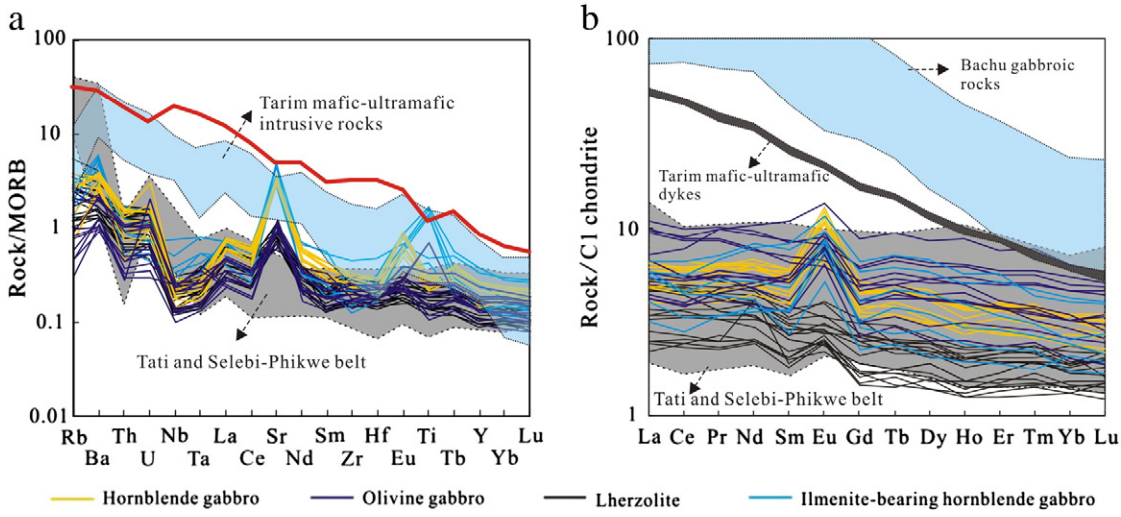

Fig. 7. (a) N-MORB normalized trace element spider diagrams and (b) C1 chondrite-normalized REE patterns of the Huangshandong intrusion. Also shown are fields for intrusive rocks from the Tati and Selebi-Phikwe belts of eastern Bostwana (Maier et al., 2008). Some data for the Huangshandong intrusion are from Deng et al. (2011a). The data for the Bachu intrusion and mafic–ultramafic dykes of the Tarim LIP are from Zhang et al. (2008) and Zhou et al. (2009). The data for N-MORB, OIB and C1 chondrite are taken from Pearce (1982) and Sun and McDonough (1989), respectively.

Table 2
Concentrations of S, Ni, Cu and PGE of the Huangshandong intrusive rocks and sulfide ores.

Location	Rock	Depth (m)	Sample	S (wt.%)	Ni (ppm)	Ir (ppb)	Ru (ppb)	Rh (ppb)	Pt (ppb)	Pd (ppb)	Cu (ppm)	Se (ppm)	Se/S ($\times 10^{-6}$)
ZK10-2	Hornblende gabbro	90	XH04-6		62.3	0.009	0.01	0.004	0.1	0.14	21.9		
	Lherzolite	180	XH04-12		543	0.03	0.038	0.15	0.5	0.36	41.8		
		210	XH04-14		546	0.018	0.035	0.014	0.48	0.22	30.7		
		240	XH04-16		630	0.024	0.054	0.016	0.66	0.41	73.2		
	Sulfide-bearing lherzolite	270	XH04-18	0.94	1677	0.13	0.15	0.085	2.49	1.6	390	1.53	163
	(Sparsely disseminated	285	XH04-19	0.35	1019	0.081	0.083	0.05	1.67	0.78	158		
	sulfide ores)	290	XH04-20	0.5	1052	0.1	0.11	0.067	1.87	1.05	179	0.57	113
		295	XH04-21	0.7	1602	0.13	0.24	0.11	2.86	2	317		
		300	XH04-22	0.59	1337	0.12	0.19	0.087	2.44	1.54	256		
		303	XH04-23	2.91	4457	0.46	0.77	0.32	9.97	4.49	1431	3.59	123
		305	XH04-24	2.9	5102	0.51	0.81	0.34	12.8	8.59	1512	3.72	128
		310	XH04-25	2.7	4555	0.45	0.84	0.56	9.98	9.69	1498		
		315	XH04-26	2.36	3459	0.43	0.78	0.36	8.37	9.29	1559	1.55	65.9
		320	XH04-27	2.78	4669	0.51	0.87	0.39	7.7	6.34	966	2.29	82.4
Samples from underground mine	Sparsely disseminated sulfide ores		XHD08-7	3.7	6271	0.65	0.93	2.13	9.23	6.1	3338		
			XHD08-14	5.04	10,226	0.79	0.59	1.24	17.1	9.31	3861	4.28	84.9
			XHD08-30	3.08	1276	0.15	0.62	0.37	6.56	5.46	24,450		
	Densely disseminated sulfide ores		XHD08-4	11.7	18,189	3.11	6.11	4.67	43.5	41.7	32,486	1.74	14.8
			XHD08-11	9.21	14,995	2.15	1.42	3.06	8.32	7.91	12,397		
			XHD08-31	6.44	9640	0.61	0.85	0.45	6.00	5.22	9676		
			XHD08-33	12.4	18,750	1.52	2.23	0.86	5.08	2.82	2474		

In summary, we propose that four pulses of magma were involved in the formation of the Huangshandong intrusion. The percentages of forsterite in olivine (68.5–82.5; Deng et al., 2012) indicate that Mg# (atomic Mg/(Fe + Mg)) of the silicate magma was less than 0.59, estimated by using a molar Mg–Fe distribution constant ($K_d = (Fe/Mg)^{Ol}/(Fe/Mg)^{magma}$) of 0.3 ± 0.03 (Roeder and Emslie, 1970). The estimated

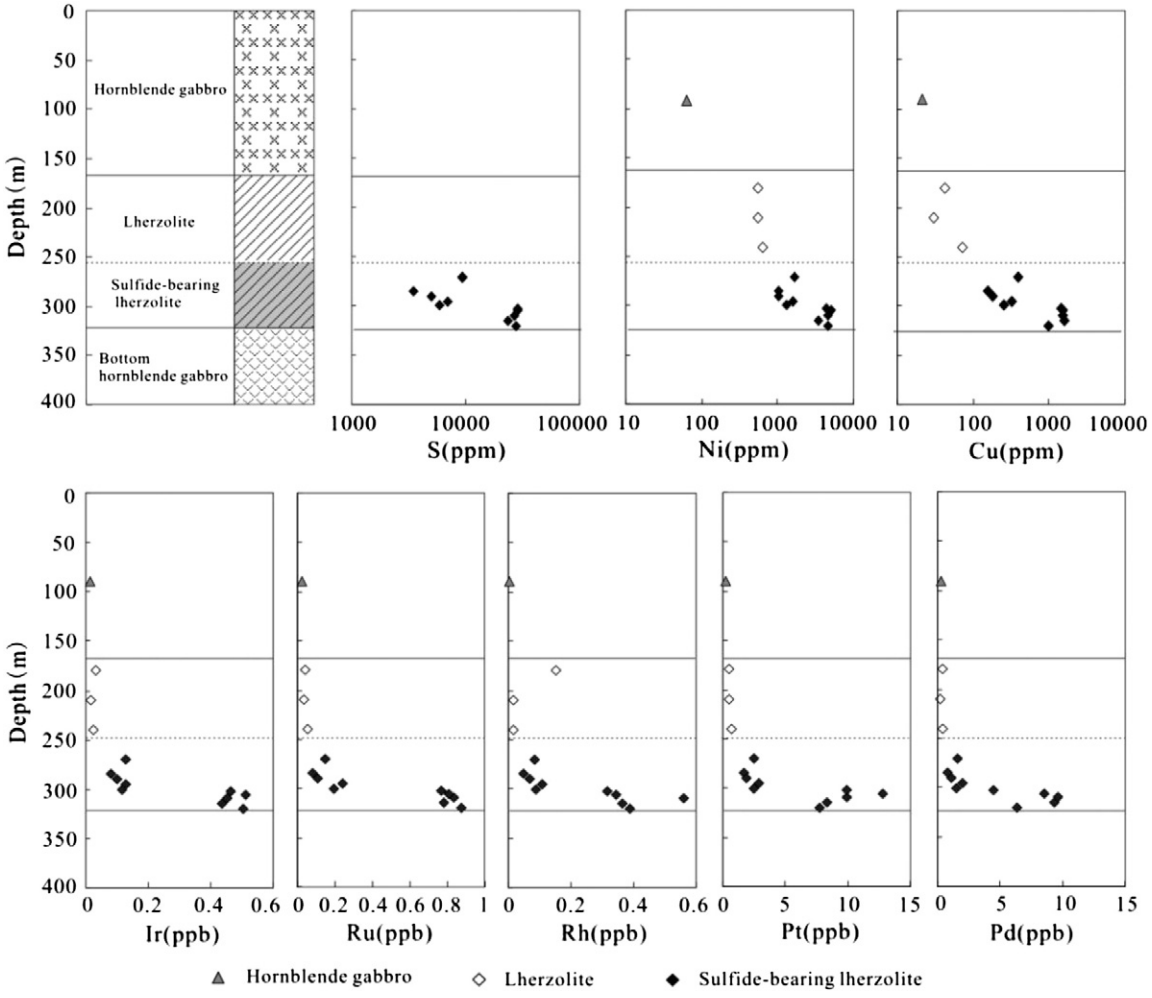

Fig. 8. Chemostratigraphic columns of S, Ni, Cu, Ir, Ru, Rh, Pt, and Pd down bore hole ZK10-2 though the Huangshandong deposit. The trends and scatter indicate that the ore metals are concentrated at the base of the lherzolite and controlled by the content of the sulfide.

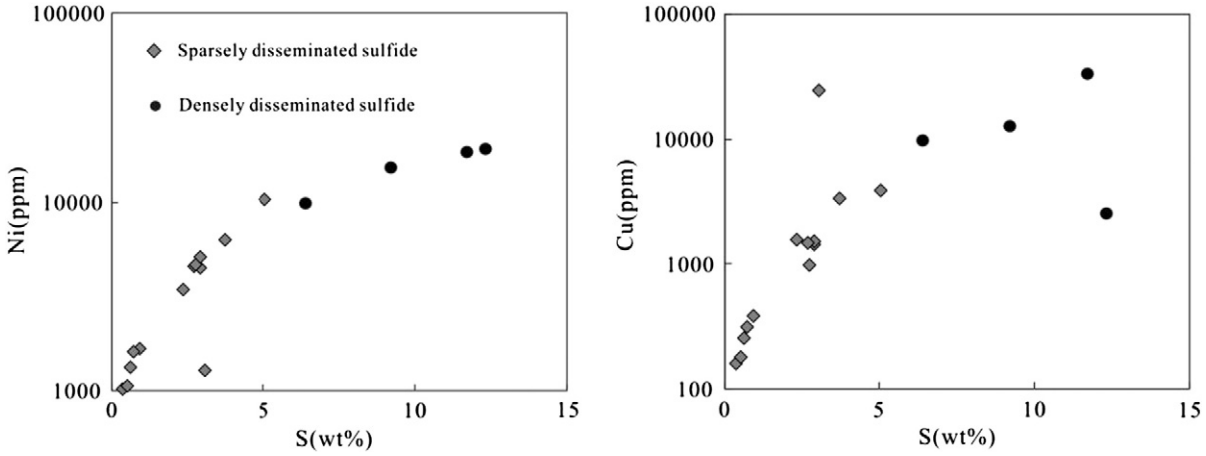

Fig. 9. Binary diagrams of Ni and Cu versus S, showing that Ni and Cu contents of the Huangshandong sulfide ores are positively correlated with S.

Mg# is much lower than that of primary magma derived from the mantle (0.68–0.75; Wilson, 1989), indicating that the magma experienced extensive evolution prior to emplacement. In addition, the trace element and PGE patterns of different types of rocks in the Huangshandong intrusion have sub-parallel trends (Fig. 7 and 10), suggesting that the different rock types are related to each other by differentiation of the same primary magma. Thus our current understanding of the intrusion is that an initial pulse of magma rose to a lower-level magma chamber and fractionated to form ultramafic cumulates and the silicate melts. They rose up at different times, accumulated in a widened part of the magma conduit and formed the Huangshandong intrusion.

6.3. Ore formation

6.3.1. Causes of sulfide saturation

When mantle-derived magma intrudes into the crust, sulfide saturation is a key process in the formation of magmatic Ni–Cu sulfide deposits. A number of experiments found that the sulfur content at sulfide saturation (SCSS) in mafic magma is mainly affected by the chemical composition, temperature, pressure, and oxygen fugacity (fO_2) of the magma (Haughton et al., 1974; Jugo, 2009; Jugo et al., 2005; Li and Ripley, 2005; Liu et al., 2007; Mavrogenes and O'Neill, 1999; Naldrett, 2009). Addition of crustal sulfur is most important for sulfide segregation and formation of magmatic Ni–Cu deposit (Keays and Lightfoot, 2010; Lesher and Keays, 2002; Lightfoot and Keays, 2005).

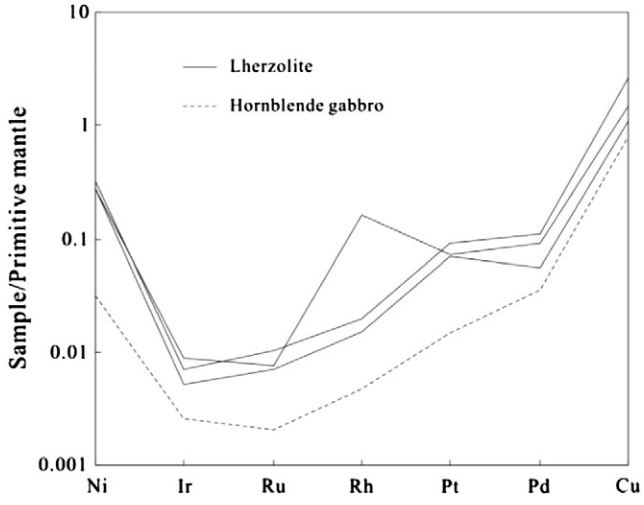

Fig. 10. Primitive mantle-normalized PGE patterns of the intrusive rocks from the Huangshandong deposit. The primitive mantle values are from Barnes and Maier (1999).

The $\delta^{34}S$ values of the Huangshandong ores are between–0.8 to 2.8‰, which are similar to those of the carbonaceous slates (1.75‰) (Wang et al., 1987). Thus the S isotopic composition alone does not constrain the role of external sulfur in the genesis of the Huangshandong deposit. Some researchers constrain the role of crustal sulfur in magmatic sulfide ores by using the Se/S ratios (Eckstrand et al., 1989; Maier et al., 2008; Ripley and Li, 2002; Theriault and Barnes, 1998). Selenium is a chalcophile element and occurs at relatively low contents in sedimentary sulfides (Peach et al., 1990). The Se/S ratios of the mantle-derived rocks are between 230 and 350 $\times 10^{-6}$, whereas crustal rocks have Se/S $<50 \times 10^{-6}$ (Eckstrand et al., 1989). Consequently, sulfides segregated from mantle magma that has assimilated crustal sulfur tend to have relatively low Se/S ratios. The Se/S ratios of the sulfide ores in the Huangshandong deposit range from 63.1 to 166 $\times 10^{-6}$ (Table 2), between the ratios of the crust and the ratios of the mantle. In addition, the negative correlation between Se/S ratios and sulfur contents in the disseminated sulfides indicate crustal contamination played a critical role for sulfide segregation of the magma (Fig. 14a). The sulfide ores from some other magmatic sulfide deposits, for which external sulfur sources have been inferred, have variable Se/S ratios, but most of them range from 50 to 300 $\times 10^{-6}$ (Fig. 14b). The Se/S ratios of the Huangshandong ores are similar to these values suggesting that the sulfide ores contain a large contribution of crustal sulfur. The initial $^{187}Os/^{188}Os$ value of 0.25 and mean γ_{Os} value of 99 in the Huangshandong sulfide ores also indicate abundant crustal contamination (Mao et al., 2002).

Magma derived from metasomatized mantle is generally characterized by high fO_2 up to QFM + 2, caused by the influx of H_2O from the subducted slab into the overlying mantle wedge (Ballhaus et al., 1991; Metrich and Clocchiatti, 1996; Parkinson and Arculus, 1999). Basaltic magmas generated in the wedge due to flux melting may have the capacity to dissolve high concentrations of sulfur as sulfate (S^{6+}) because of the high fO_2 conditions (Jugo et al., 2005). It has been proved that reduction of the magma by assimilation of crustal graphite plays a key role in sulfide saturation in some large Ni–Cu sulfide deposits (Li et al., 2003; Ripley et al., 2007; Song et al., 2011b; Thakurta et al., 2008; Tomkins et al., 2012). A layer of graphite (0.6–1 m thick, 1.5 km long) occurs in the Gandun formation in the Huangshan area (Wang et al., 1987). The carbonaceous slates containing graphite changed into graphite–sericite–quartz hornfels through thermal metamorphism along the margins of the Huangshandong intrusion, and carbonaceous slate xenoliths are found enclosed in the hornblende gabbro, suggesting that the magma assimilated the graphite (Wang et al., 1987). Thus, assimilation

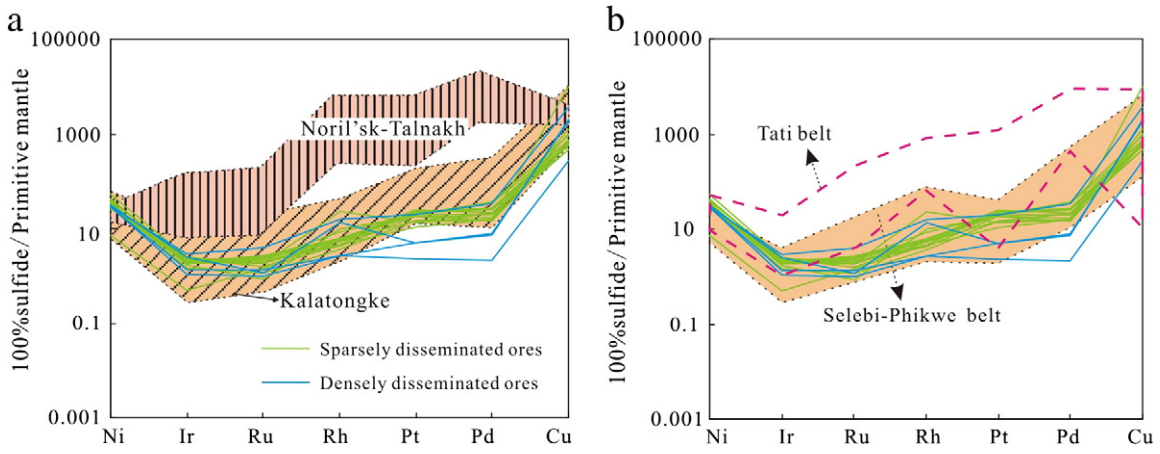

Fig. 11. Sulfide ores (on 100% sulfide basis) of the Huangshandong deposit normalized to the primitive mantle (Barnes and Maier, 1999). Data for Noril'sk-Talnakh and Kalatongke are from Naldrett (2004) and Song and Li (2009). The data for the sulfide ores from Tati and Selebi-Phikwe belts of eastern Bostwana are from Maier et al. (2008).

of crustal graphite in the Gandun formation may have caused the reduction of the oxidized magma, which was accompanied by a sharp decrease in S solubility thereby accelerating the onset of saturation.

6.3.2. Origin of PGE-depleted sulfide mineralization

The cause of PGE depletion of the sulfide ores in the Ni–Cu deposits in north Xinjiang is a matter of debate. Some researchers propose previous sulfide segregation during magma ascent or storage at depth (Song and Li, 2009; Tang et al., 2011; Yang et al., 2012). However, some other researchers suggested that PGE depletion in the primary magma can be explained by a relatively low degree of partial melting of the mantle and retention of coexisting sulfide liquid in the mantle (Li et al., 2012).

It is well known that PGE are strongly concentrated in sulfides in the mantle, whereas, when magmas are generated at $fO_2 \geq FMQ + 2$ in the mantle, Cu, Au and PGE may be enriched in the silicate magma even under low degrees of partial melting because the sulfides are replaced by sulfates (Jugo et al., 2005; Mungall et al., 2006). On the Pd/Ir vs Ni/Cu diagram (Fig. 12), the Huangshandong samples plot in the field of high-Mg basalts and layered intrusions, indicating a moderate degree of partial melting of the mantle. Thus, the primary magma of the Huangshandong intrusion derived from metasomatized mantle was probably not depleted in PGE under relatively high oxygen fugacity due to the occurrence of H_2O in the mantle source.

Metal contents of sulfide melts segregated from silicate magma are a function of the R factors and the metal partition coefficients (Campbell and Naldrett, 1979):

$$C_i^{sul} = C_i^{sil} * D_i * (R + 1)/(R + D_i) \quad (1)$$

where C_i^{sul} and C_i^{sil} represent the content of element i in the sulfide liquid and in the parental silicate liquid, respectively, D_i is the partition coefficient of element i between sulfide liquid and silicate liquid, and R is the R factor.

As noted above, the geochemical signatures of the Huangshandong intrusion are similar to these of island arc magmas, which have 45 ppm Cu and 7.5 ppb Pd (Barnes et al., 1993). It is assumed that the partition coefficients of Pd and Cu between the sulfide and silicate liquid are 40,000 and 1000 (Fleet et al., 1993; Francis, 1990). The Huangshandong sulfides have lower Pd content and higher Cu/Pd ratios than the modeled values to be separated from the metal-undepleted island arc magma (Fig. 15), indicating that the Huangshandong sulfides were separated from a parental magma strongly depleted in PGE. Calculations according to Rayleigh's Law indicate that 0.012% sulfide melt removal from the island arc magma would give rise to a residual magma with 39.9 ppm Cu and 0.06 ppb Pd. The sulfides plot on the 0.012% earlier sulfide removal line, with R factor ranging from 100 to 3000 (Fig. 15), suggesting that the Huangshandong sulfides were segregated from a PGE-depleted parental magma that experienced earlier sulfide segregation during magma ascent or storage at depth. Densely disseminated sulfides were segregated from the PGE-depleted magma at lower R factor values and thus have a lower Pd content than the sparsely disseminated sulfides. In addition, the Pd contents and Cu/Pd ratios of the Huangshandong ores are similar to those of the Selebi-Phikwe belt ores and different from those of the Tati ores of eastern Botswana (Fig. 15). The former is interpreted to be formed by sulfide segregation from a strongly PGE-depleted magma that experienced early sulfide removal, and the latter was directly segregated from undepleted island arc magma (Maier et al., 2008).

Thus, we propose that PGE depletion in the sulfides of the Huangshandong deposit was due to sulfide segregation at depth, rather than resulting from the occurrence of sulfides in the mantle.

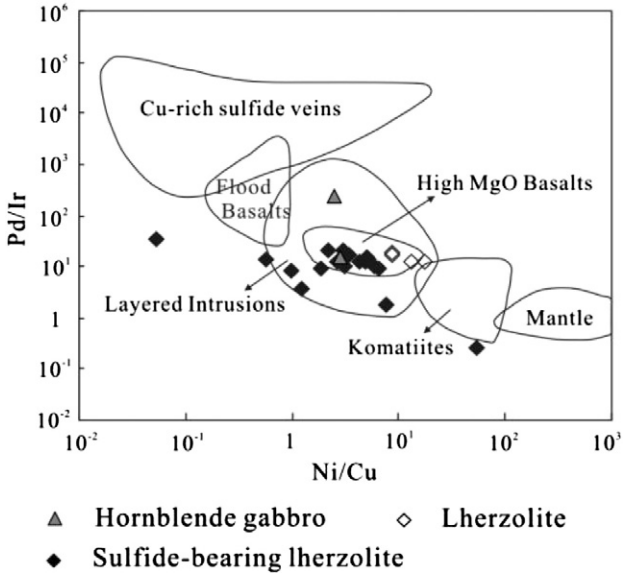

Fig. 12. Diagram of Pd/Ir versus Ni/Cu, showing that the Huangshandong intrusive rocks and sulfide ores are associated with basaltic magma (Barnes and Lightfoot, 2005).

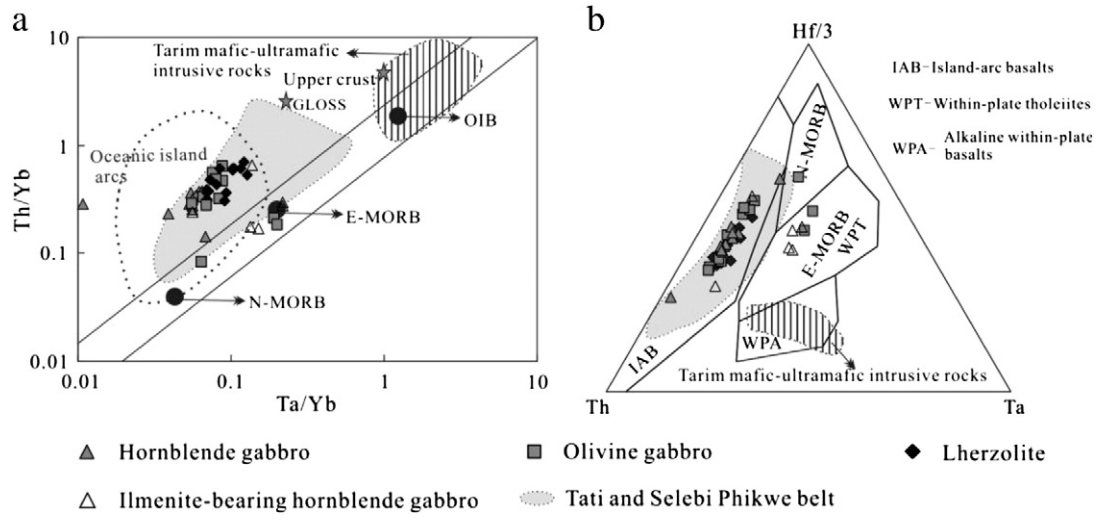

Fig. 13. (a) Th/Yb vs. Ta/Yb plot showing that the Huangshandong intrusive rocks plot within the fields of oceanic island arc, above the MORB-OIB array. Fields of oceanic island arc and active continental margins are after Pearce (1983), data for MORB and OIB are from Pearce (1982) and Sun and McDonough (1989), data for crust and global subducting sediment (GLOSS) are from Rudnick and Fountain (1995) and Plank and Langmuir (1998), respectively. (b) Th–Hf–Nb discrimination diagram showing that the Huangshandong intrusive rocks plot within the fields of island-arc basalts. Some data for the Huangshandong intrusion are from Deng et al. (2011a). Data for Tati and Selebi-Phikwe belt are from Maier et al. (2008). Data for Tarim mafic–ultramafic rocks are from Zhang et al. (2008) and Zhou et al. (2009).

6.3.3. Crystal fractionation of sulfide melt

Because all PGEs are compatible in sulfide melts, sulfide melt segregation and reaction with fresh magma cause slight differentiation of these metals. However, palladium and platinum are incompatible in monosulfide solid solution (MSS), which is the first phase to crystallize from sulfide melt, whereas iridium–platinum group elements are compatible in MSS (Barnes et al., 1997; Fleet et al., 1993; Kullerud et al., 1969; Naldrett et al., 1967). Thus, fractionation of sulfide melts has played an important role in the composition variations of sulfide ores. In the model calculations in this study, we assume D_{Pd}, D_{Ir}, D_{Ni} between MSS and sulfide melt to be 0.1, 5, and 0.8 respectively. MSS is the fractionating phase.

Sulfide melts separated from a PGE-depleted parental magma containing 0.06 ppb Pd, 0.002 ppb Ir, and 132 ppm Ni under an R-factor of 3000 would contain 172 ppb Pd, 5.22 ppb Ir, and 56,531 ppm Ni. According to the calculation of sulfide fractionation shown in Fig. 16, most of the Huangshandong sparsely disseminated sulfides plot on the trend of crystallization of MSS (Model 1 cumulates), while the densely disseminated sulfides plot on the trend of fractional crystallization (Model 2 cumulates). Because the MSS cumulates have Pd/Ir lower than the initial values of the original sulfide melts (Song et al., 2008), the low Pd/Ir ratios indicate that the densely disseminated sulfides accumulated more MSS compared to the sparsely disseminated sulfides (Fig. 16). In addition, the relatively constant Pd/Ir ratios of some Huangshandong sparsely disseminated sulfides suggest that these sulfides continuously reacted with fresh magma and were not modified by fractionation. As the sulfide melt/silicate liquid partitioning coefficient of Ir is much higher than that of Ni (Fleet et al., 1993; Francis, 1990), it is apparent that the densely disseminated sulfides were segregated from the PGE-depleted magma at lower R factor values and thus

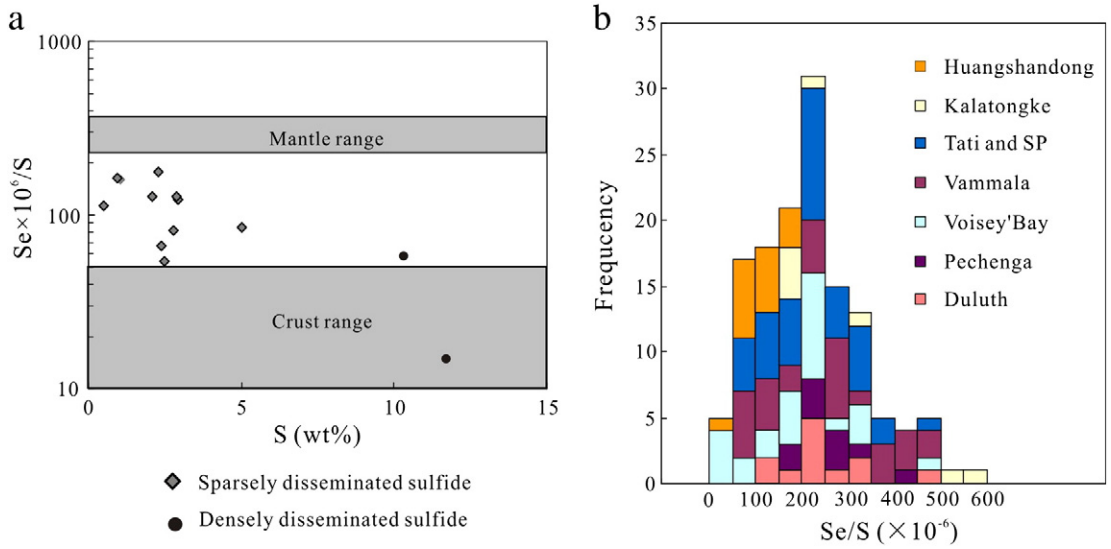

Fig. 14. (a) Se/S vs. S for the Huangshandong sulfide ores. Range in Se/S ratio of the mantle and crust is taken from Eckstrand et al. (1989). (b) Se/S frequency histogram of sulfide ores from Huangshandong and some other magmatic sulfide deposits. Data for Kalatongke, Vammala, Voisey's Bay, Pechenga, Dunka Road, Tati and Selebi-Phikwe (SP) belt are from Zhang et al. (2009), Peltonen (1995a), Ripley and Li (2002), Barnes et al. (2001), Theriault and Barnes (1998), and Maier et al. (2008).

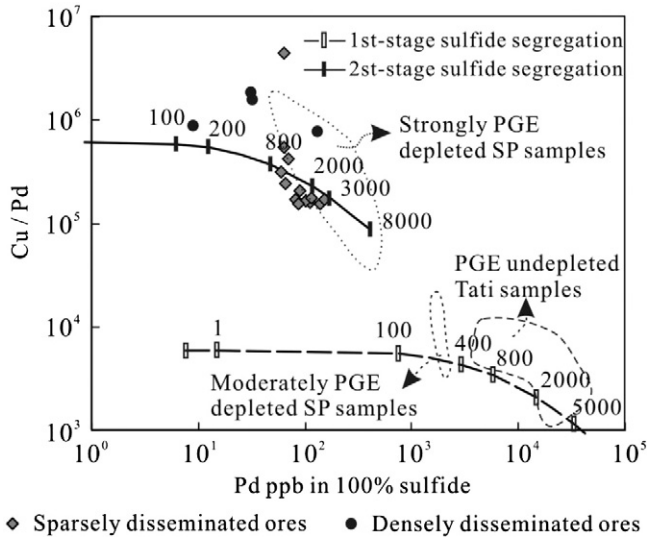

Fig. 15. Cu/Pd vs Pd of sulfide ores in the Huangshandong deposit. Tie lines of 1st-stage sulfide segregation are drawn for model sulfides separating from metal-undepleted island arc magma (45 ppm Cu, 7.5 ppb Pd; Barnes et al., 1993) at variable R factors. Tie lines of 2nd-stage sulfide segregation are drawn for model sulfides separating from a PGE-depleted magma with 39.9 ppm Cu and 0.06 ppb Pd at variable R factors (because of 0.012% sulfide removal from magma). The Huangshandong samples have high Cu/Pd ratios, similar to the strongly PGE-depleted Selebi-Phikwe samples, indicating the parental magma experienced early sulfide removal. The data for Tati and Selebi-Phikwe belt are from Maier et al. (2008).

contain higher Ni/Ir ratios (5.85×10^7–15.7×10^7) than those of the sparsely disseminated sulfides (1.18×10^7–13.0×10^7).

6.4. Exploration potential in orogenic belts

In past decades increasing numbers of magmatic sulfide deposits have been found in orogenic belts, such as Vammala Ni belt (Finland), Aguablanca (Spain), Hongqiling (China), Quetico (Canada), Duck Island (USA), Tati and Selebi-Phikwe belts (Botswana), Kalatongke (NW China) (Li et al., 2012; Maier et al., 2008; Peltonen, 1995a; Pettigrew and Hattori, 2006; Ripley, 2009; Thakurta et al., 2008; Tornos et al., 2001; Wu et al., 2004), indicating significant exploration potential in these tectonic settings.

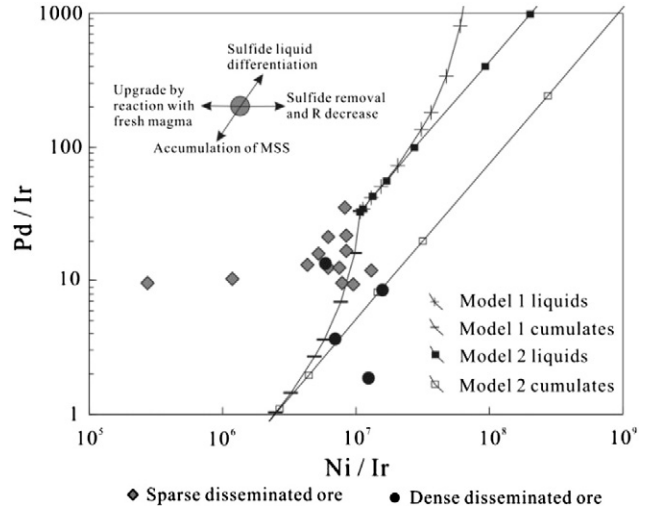

Fig. 16. Model calculation for fractional and equilibrium crystallization of MSS from sulfide liquids in the Huangshandong sulfide deposit. Liquid and cumulate trends are calculated using the Rayleigh equation or equilibrium crystallization equation. Models 1 and 2 show the trends of equilibrium and fractional crystallization of the Ni–Cu sulfides, respectively. Pd/Ir and Ni/Ir ratios of the Huangshandong sulfides are consistent with Model 1 cumulates, suggesting that the differentiation of the Huangshandong sulfides was controlled dominantly by equilibrium crystallization of MSS.

Recent simulation shows that contamination of only 0.14 wt.% C could decrease the oxygen fugacity of the magma from FMQ + 2 to FMQ, leading to sulfur saturation (Thakurta et al., 2008). Deep-sea sediments always have high carbon contents because of high organic productivity in the overlying waters, high input of terrigenous organic matter, and rapid burial rate (e.g. in turbidites; Stein, 1990). Thus, assimilation of crustal S and graphite in orogenic belts would result in sulfide saturation of the magma and segregation of immiscible sulfide. Many researchers regard the intrusions in orogenic belts as a key part of conduit systems (Irvine, 1974; Murray, 1972; Peltonen, 1995b; Tornos et al., 2006; Zhang et al., 2011). The immiscible sulfides in magma tend to be deposited due to a sudden decrease of magma velocity in response to increase in conduit size. When the metal-undepleted magma flows through the sulfides that are lodged in traps in the conduit, it would interact with the sulfides, upgrading them in chalcophile elements.

In summary, mafic magma derived from metasomatized mantle in orogenic belts could meet the requirements necessary for sulfide segregation and accumulation when they ascend to the crust and generate Ni–Cu sulfide deposits. As exploration and research has been carried out, several economic Ni–Cu deposits have been found in northern Xinjiang (such as the Tianyu, Baishiquan, Tulaergen and the large scale Pobei Ni–Cu deposit) (Sun et al., 2006; Chai et al., 2008; San et al., 2010). Identification of an increasing number of sizeable magmatic Ni–Cu deposits in orogenic environments suggests the mafic–ultramafic intrusions in orogenic belts should be regarded as favorable exploration targets.

7. Conclusions

The primary magma of the Huangshandong intrusion was generated by partial melting of a metasomatized mantle modified by subducted slab-derived melt/fluid. Four pulses of magma were involved in the formation of the Huangshandong intrusion. Assimilation of crustal S and graphite played a critical role in producing sulfide saturation in the parental magma of the deposit. We propose that PGE depletion in the sulfides of the Huangshandong deposit is due to previous sulfide segregation at depth, other than retention of coexisting sulfide in the mantle. The low Pd/Ir and high Ni/Ir ratios suggest that the densely disseminated sulfides were segregated from the PGE-depleted magma at lower R factor values and accumulated more monosulfide solid solution compared to the sparsely disseminated sulfides.

Acknowledgments

We thank the management of No. 6 Geological Team of Xinjiang Bureau of Geology and Mineral Resources for help during our field work. We also thank Liang Qi, Wenqin Zheng, Jing Hu for their assistance with laboratory work. Comments from N C. White have improved the manuscript. Constructive reviews from anonymous reviewers are appreciated. This study was financially supported by the Research Fund of the State Key Laboratory of Ore Deposit Geochemistry (SKLOG-ZY125-06), the Chinese National Science and Technology Program during the 12th Five-year Plan Period (2011BAB06B01), the Program for New Century Excellent Talents in University (Grant no. NCET-10-0324), NSFC research grants (40973038, 41172090, 41040025, 41303031) and Open Funds from the State Key Laboratory of Ore Deposit Geochemistry, Institute of Geochemistry, Chinese Academy of Sciences (201102).

References

Aldanmaz, E., Pearce, J.A., Thirlwall, M.F., Mitchell, J.G., 2000. Petrogenetic evolution of late Cenozoic, post-collision volcanism in western Anatolia, Turkey. J. Volcanol. Geotherm. Res. 102 (1–2), 67–95.

Asif, M., Parry, S.J., 1991. Study of the digestion of chromite during nickel sulphide fire assay for the platium group elements and gold. Analyst 116, 1071–1073.

Ballhaus, C.R., Berry, B.F., Green, D.H., 1991. High pressure experimental calibration of the olivine–orthopyroxene–spinel oxygen geobarometer: implications for the oxidation state of the upper mantle. Contrib. Mineral. Petrol. 107 (1), 27–40.

Barnes, S.J., Lightfoot, P.C., 2005. Formation of magmatic nickel sulfide group ore deposits and processes affecting their copper and platinum-group element contents. Economic Geology 100th Anniversary Volume 179–213.

Barnes, S.J., Maier, W.D., 1999. The fractionation of Ni, Cu, and the noble metals in silicate and sulfide liquids. In: Keays, R.R., Lesher, C.M., Lightfoot, P.C., Farrow, C.E.G. (Eds.), Dynamic Processes in Magmatic Ore Deposits and their Application to Mineral Exploration. Geological Association of Canada, Short course notes, 13, pp. 69–106.

Barnes, S.J., Couture, J.F., Sawyer, E.W., Bouchaib, C., 1993. Nickel–copper occurrences in the Belleterre–Angliers belt of the Pontiac Subprovince and the use of Cu–Pd ratios in interpreting platinum-group element distributions. Econ. Geol. 88, 1402–1419.

Barnes, S.J., Makovicky, E., Makovicky, M., Hansen, J.R., Moller, S.K., 1997. Partition coefficients for Ni, Cu, Pd, Pt, Rh and Ir between monosulfide solid solution and sulfide liquid and the implication for the formation of compositionally zoned Ni–Cu sulfide bodies by fractional crystallization of sulfide liquid. Can. J. Earth Sci. 34, 366–374.

Barnes, S.J., Melezhik, V.A., Sokolov, S.V., 2001. The composition and mode of formation of the Pechenga nickel deposits, Kola Peninsula, Northwestern Russia. Can. Mineral. 39 (2), 447–471.

Begg, G.C., Hronsky, J.A.M., Arndt, N.T., Griffin, W.L., O'Reilly, S.Y., Hayward, N., 2010. Lithospheric, cratonic and geodynamic setting of Ni–Cu–PGE sulfide deposits. Econ. Geol. 105, 1057–1070.

BGMX, 1993. Regional Geology of Xinjiang Uygur Autonomous Region. Geological Publishing House, Beijing 1–841 (in Chinese with English abstract).

Campbell, I.H., Naldrett, A.J., 1979. The influence of silicate: sulfide ratios on the geochemistry of magmatic sulfides. Econ. Geol. 74, 1503–1506.

Cesare, B., Rubatto, D., Hermann, J., Barzi, L., 2002. Evidence for Late Carboniferous subduction-type magmatism in mafic–ultramafic cumulates of the SW Tauern window (Eastern Alps). Contrib. Mineral. Petrol. 142 (4), 449–464.

Chai, F.M., Zhang, Z.C., Mao, J.W., Dong, L.H., Zhang, Z.H., Wu, H., 2008. Geology, petrology and geochemistry of the Baishiquan Ni–Cu-bearing mafic–ultramafic intrusions in Xinjiang, NW China: implications for tectonics and genesis of ores. J. Asian Earth Sci. 32 (2–4), 218–235.

Chen, F.W., Li, H.Q., Chen, Y.C., Wang, D.H., Wang, J.L., Liu, D.Q., Tang, Y.L., Zhou, R.H., 2005. Zircon SHRIMP U–pb dating and its geological significance of mineralization in Tuwu–Yandong Porphyry Copper Mine, East Tianshan Mountain. Acta Geol. Sin. 79 (2), 256–261 (in Chinese with English abstract).

Chen, X.J., Shu, L.S., Santosh, M., Zhao, X.X., 2013. Island arc-type bimodal magmatism in the eastern Tianshan Belt, Northwest China: geochemistry, zircon U–Pb geochronology and implications for the Paleozoic crustal evolution in Central Asia. Lithos 168–169, 48–66.

Cottin, J.Y., Lorand, J.P., Agrinier, P., Bodinier, J.L., Liegeois, J.P., 1998. Isotopic (O, Sr, Nd) and trace element geochemistry of the Laouni layered intrusions (Pan-African belt, Hoggar, Algeria): evidence for post-collisional continental tholeiitic magmas variably contaminated by continental crust. Lithos 45 (1–4), 197–222.

Deng, Y.F., Song, X.Y., Jie, W., Chen, S.L., Li, J., 2011a. Petrogenesis of the Huangshandong Ni-Cu sulfide-bearing mafic–ultramafic intrusion, Northern Tianshan, Xinjiang: evidence from major and trace elements and Sr–Nd isotope. Acta Geol. Sin. 85 (9), 1436–1451 (in Chinese with English abstract).

Deng, Y.F., Song, X.Y., Chen, L.M., Cheng, S.L., Zhang, X.L., Li, J., 2011b. Features of the mantle source of the Huangshanxi Ni–Cu sulfide-bearing mafic–ultramafic intrusion, eastern Tianshan. Acta Petrol. Sin. 27 (12), 3640–3652 (in Chinese with English abstract).

Deng, Y.F., Song, X.Y., Zhou, T.F., Yuan, F., Chen, L.M., Zheng, W.Q., 2012. Correlations between Fo number and Ni content of olivine of the Huangshandong intrusion, eastern Tianshan, Xinjiang, and genetic significances. Acta Petrol. Sin. 28 (7), 2224–2234 (in Chinese with English abstract).

Djafer, S.A., Ouzegane, K., Liegeois, J.P., Kienast, J.R., 2003. An example of post-collisional mafic magmatism: the gabbro–anorthosite layered complex from the Tin Zebane area (western Hoggar, Algeria). J. Afr. Earth Sci. 37, 313–330.

Eckstrand, O., Grinenko, L., Krouse, H., Paktunc, A., Schwann, P., Scoates, R., 1989. Preliminary data on sulphur isotopes and Se/S ratios, and the source of sulphur in magmatic sulphides from the Fox River Sill, Molson Dykes and Thompson nickel deposits, northern Manitoba1. Current Research Part:C, Geological Survey of Canada. Paper, 89-1C, pp. 235–242.

Fleet, M.E., Chryssoulis, S.L., Stone, W.E., Weisener, C.G., 1993. Partition of platinum-group elements and Au in the Fe–Ni–Cu–S system: experiments on the fractional crystallization of sulfide melt. Contrib. Mineral. Petrol. 115 (1), 36–44.

Francis, R.D., 1990. Sulfide globules in mid-ocean ridge basalts (MORB) and the effect of oxygen abundance in Fe–S–O on the ability of those liquids to partition metals from MORB and komatiitic magmas. Chem. Geol. 85 (3–4), 199–213.

Gu, L.X., Hu, S.X., Yu, C.S., Wu, C.Z., Yan, Z.F., 2001. Initiation and evolution of the Bogda subduefion-torn-type rift. Acta Petrol. Sin. 17 (4), 585–597 (in Chinese with English abstract).

Gu, L.X., Zhang, Z.Z., Wu, C.Z., Wang, Y.X., Tang, J.H., Wang, C.S., Xi, A.H., Zheng, Y.C., 2006. Some problems on granitesand vertical growth of the continental crust in the eastern Tianshan Mountains, NW China. Acta Petrol. Sin. 22 (5), 1103–1120 (in Chinese with English abstract).

Han, B.F., Ji, J.Q., Song, B., Chen, L.H., Li, Z.H., 2004. Zircon SHRIMP U–Pb age and geology of Kalatongke–Huangshan mafic–ultramafic complex, Xinjiang, China. Chin. Sci. Bull. 49 (22), 2324–2328 (in Chinese with English abstract).

Han, C.M., Xiao, W.J., Zhao, G.C., Mao, J.W., Yang, J.M., Wang, Z.L., Yan, Z., Mao, Q.G., 2006. Geological characteristics and genesis of the Tuwu porphyry copper deposit, Hami, Xinjiang, Central Asia. Ore Geol. Rev. 29, 77–94.

Han, C.M., Xiao, W.J., Zhao, G.C., Ao, S.J., Zhang, J.E., Qu, W.J., Du, A.D., 2010. In-situ U–Pb, Hf and Re–Os isotopic analyses of the Xiangshan Ni–Cu–Co deposit in Eastern Tianshan (Xinjiang), Central Asia Orogenic Belt: Constraints on the timing and genesis of the mineralization. Lithos 120, 547–562.

Haughton, D., Roeder, P., Skinner, B., 1974. Solubility of sulfur in mafic magmas. Econ. Geol. 69 (4), 451–467.

Hawkesworth, C.J., O'Nions, R.K., Pankhurst, R.J., Hamilton, P.J., Evensen, N.M., 1977. A geochemical study of island arc and back-arc tholeiites from the Scotia Sea. Earth Planet. Sci. Lett. 36, 253–262.

Himmelberg, G.R., Loney, R.A., 1995. Characteristics and petrogenesis of Alaskan-type ultramafic–mafic intrusions, southern Alaska. USGS Prof Paper 1564, 0-47.

Hong, D.W., Zhang, J.S., Wang, T., Wang, S.G., Xie, X.L., 2004. Continental crustal growth and the supercontinental cycle: evidence from the Central Asian Orogenic Belt. J. Asian Earth Sci. 23 (5), 799–813.

Hou, G.S., Tang, H.F., Liu, C.Q., 2006. Geochemical characteristics of the Late Paleozoic Volcanics in Jueluotage tectonic belt, eastern Tianshan and its implications. Acta Petrol. Sin. 22 (5), 1167–1177 (in Chinese with English abstract).

Hu, P.Q., Ren, L.Y., Fu, P.E., Zhang, M.J., Li, X.Y., Qin, H.Y., 2010. Petrogenetic and ore-forming processes of Huangshandong Cu–Ni sulfide deposit in Hami Xinjiang. Miner. Depos. 29, 158–168 (in Chinese with English abstract).

Irvine, T., 1974. Petrology of the Duke Island ultramafic complex, southeastern Alaska. Geol. Soc. Am. Mem. 138, 1–240.

Jahn, B.M., Wu, F.Y., Chen, B., 2000. Massive granitoid generation in Central Asia: Nd isotope evidence and implication for continental growth in the Phanerozoic. Episodes 23 (2), 82–92.

Ji, J.S., Li, H.Q., Zhang, L.C., 1999. Sm–Nd and Rb–Sr isotopic ages of magnetite–chlorite formation gold deposit in the volcanic rock area of Late Paleozoic Era, East Tianshan. Chin. Sci. Bull. 44 (19), 1801–1804.

Johnson, M.C., Plank, T., 1999. Dehydration and melting experiments constrain the fate of subducted sediments. Geochem. Geophys. Geosyst. 1 (12). http://dx.doi.org/10.1029/1999GC000014.

Jugo, P., 2009. Sulfur content at sulfide saturation in oxidized magmas. Geology 37 (5), 415–418.

Jugo, P., Luth, R., Richards, J., 2005. Experimental data on the speciation of sulfur as a function of oxygen fugacity in basaltic melts. Geochim. Cosmochim. Acta 69 (2), 497–503.

Keays, R.R., Lightfoot, P.C., 2010. Crustal sulfur is required to form magmatic Ni–Cu sulfide deposits: evidence from chalcophile element signatures of Siberian and Deccan Trap basalts. Miner. Deposita 45 (3), 241–257.

Kullerud, G., Yund, R.A., Moh, G.H., 1969. Phase relations in the Cu–Fe–S, Cu–Ni–S and Fe–Ni–S systems. Econ. Geol. 4, 323–343.

Lesher, C.M., Keays, R.R., 2002. Komatiite-associated Ni–Cu–(PGE) deposits: geology, mineralogy, geochemistry and genesis. In: Cabri, L. (Ed.), The Geology, Geochemistry, Mineralogy and Beneficiation of the Platinum-group Elements. Canadian Institute of Mining, Metallurgy and Petroleum Special Volume, 54, pp. 579–617.

Li, C.S., Ripley, E.M., 2005. Empirical equations to predict the sulfur content of mafic magmas at sulfide saturation and applications to magmatic sulfide deposits. Miner. Deposita 40 (2), 218–230.

Li, D.H., Bao, X., Zhang, B., Han, Z., Lan, G., Zheng, Z., et al., 1989. Investigation of geology, geophisics and geochemistry of the Huangshan–Cu–Ni metallogenic belt for mineral exploration, unpublished report by National 305 project office in Xinjiang. 0–418 (in Chinese).

Li, C.S., Ripley, E.M., Naldrett, A.J., 2003. Compositional variations of olivine and sulfur isotopes in the Noril'sk and Talnakh intrusions, Siberia: implications for ore-forming processes in dynamic magma conduits. Econ. Geol. 98 (1), 69–86.

Li, X.M., Xia, L.Q., Xia, Z.C., Xu, X.Y., Ma, Z.P., Wang, L.S., 2004. Zircon U–Pb geochronology of volcanic rocks of the Qi'eshan Group in the East Tianshan Mountains. Geol. Bull. China 23 (12), 1215–1220 (in Chinese with English abstract).

Li, X.H., Su, L., Chung, S.L., Li, X.Z., Liu, Y., Song, B., Liu, D.Y., 2005. Formaton of the Jinchuan ultramafic intrusion and the world's third largest Ni–Cu sulfide deposit: Associated with the similar to 825 Ma South China mantle plume. Geochem. Geophys. Geosyst. 6 (11), Q1104. http://dx.doi.org/10:1029/2005GC001006.

Li, J.Y., Wang, K.Z., Sun, G.H., Mo, S.G., Li, W.Q., Yang, T.N., Gao, L.M., 2006a. Paleozoic active margin slices in the southern Turfan Hami basin: geological records of subduction of the Paleo Asian Ocean plate in central Asian regions. Acta Petrol. Sin. 22 (5), 1087–1102 (in Chinese with English abstract).

Li, J.Y., Song, B., Wang, K.Z., Li, Y.P., Sun, G.H., Qi, D.Y., 2006b. Permian mafic–ultramafic complexes on the Southern margin of the Tu-Ha basin, east Tianshan mountains: geological records of vertical crustal growth in Central Asia. Acta Geosci. Sin. 27 (5), 424–446 (in Chinese with English abstract).

Li, W.Q., Xia, B., Wang, K.Z., Wang, Q., Wang, H., 2006c. Zircon SHRIMP age and geochemistry of Caizhong Granite from East Tianshan, Xinjiang, China. Acta Geol. Sin. 80 (1), 43–52 (in Chinese with English abstract).

Li, C.S., Zhang, M.J., Fu, P.E., Qian, Z.Z., Hu, P.Q., Ripley, E.M., 2012. The Kalatongke magmatic Ni–Cu deposits in the Central Asian Orogenic Belt, NW China: product of slab window magmatism? Miner. Deposita 47 (1–2), 51–67.

Lightfoot, P.C., Keays, R.R., 2005. Siderophile and chalcophile metal variations in flood basalts from the Siberian Trap, Noril'sk Region: implications for the origin of the Ni–Cu–PGE sulfide ores. Econ. Geol. 100 (3), 439–462.

Liu, W., Fei, P.X., 2006. Methane-rich fluid inclusions from ophiolitic dunite and post-collisional mafic–ultramafic intrusion: the mantle dynamics underneath the Palaeo-

Asian Ocean through to the post-collisional period. Earth Planet. Sci. Lett. 242, 286–301.
Liu, D.Q., Tang, Y.L., Zhou, R.H., 2005. Copper Deposits and Nickel Deposits in Xinjiang. Geological Publishing House, China. Beijing 1–360 (in Chinese with English abstract).
Liu, Y., Samaha, N.T., Baker, D.R., 2007. Sulfur concentration at sulfide saturation (SCSS) in magmatic silicate melts. Geochim. Cosmochim. Acta 71 (7), 1783–1799.
Ma, R.S., Wang, C.Y., Ye, S.F., Liu, G.B., 1993. Tectonic framework and crustal evolution of the Eastern Tianshan. Nanjing University Press (in Chinese).
Maier, W.D., Barnes, S.J., Chinyepi, G., Barton, J.J., Eglington, B., Setshedi, T., 2008. The composition of magmatic Ni–Cu–(PGE) sulfide deposits in the Tati and Selebi-Phikwe belts of eastern Botswana. Miner. Deposita 43 (1), 37–60.
Mao, J.W., Yang, J.M., Qu, W.J., Du, A.D., Wang, Z.L., Han, C.M., 2002. Re–Os dating of Cu–Ni sulfide ores from Huangshandong deposit in Xinjiang and its geodynamic significance. Miner. Depos. 21 (4), 323–330 (in Chinese with English abstract).
Mao, J.W., Pirajno, F., Zhang, Z.H., Chai, F.M., Wu, H., Chen, S.P., Chen, L.S., Yang, J.M., Zhang, C.Q., 2008. A review of the Cu–Ni sulphide deposits in the Chinese Tianshan and Altay orogens (Xinjiang Autonomous Region, NW China): Principal characteristics and ore-forming processes. J. Asian Earth Sci. 32 (2–4), 184–203.
Mavrogenes, J.A., O'Neill, H.S.C., 1999. The relative effects of pressure, temperature and oxygen fugacity on the solubility of sulfide in mafic magmas. Geochim. Cosmochim. Acta 63 (7–8), 1173–1180.
Metrich, N.M., Clocchiatti, R., 1996. Sulfur abundance and its speciation in oxidized alkaline melts. Geochim. Cosmochim. Acta 60 (21), 4151–4160.
Mungall, J., Hanley, J., Arndt, N., Debecdelievre, A., 2006. Evidence from meimechites and other low-degree mantle melts for redox controls on mantle–crust fractionation of platinum-group elements. Proc. Natl. Acad. Sci. 103 (34), 12695–12700.
Murray, C.G., 1972. Zoned ultramafic complexes of the Alaskan type: feeder pipes of andesitic volcanoes. In: Shagam, R.E., et al. (Ed.), Studies in earth and space science (Hess Volume). Geologic society of America Memoir, 132, pp. 313–335.
Naldrett, A.J., 2004. Magmatic Sulfide Deposits: Geology, Geochemistry and Exploration. Springer, Verlaag 1–728.
Naldrett, A.J., 2009. Fundamentals of magmatic sulfide deposits. In: Li, C., Edward, M.R. (Eds.), New Developments in Magmatic Ni–Cu and PGE Deposits. , 1. Geological Publishing House, Beijing, pp. 1–26.
Naldrett, A.J., Craig, J.R., Kullerud, G., 1967. The central potion of the Fe–Ni–S system and its bearing on pentlandite solution in iron–nickel sulfide ores. Econ. Geol. 62, 826–847.
Naldrett, A.J., Fedorenko, V., Lightfoot, P., Kunilov, V., Gorbachev, N., Doherty, W., Johan, Z., 1995. Ni–Cu–PGE deposits of the Noril'sk region, Siberia: Their formation in conduits for flood basalt volcanism. Inst. Min. Metall., Sect. B 104, 18–36.
Parkinson, I.J., Arculus, R.J., 1999. The redox state of subduction zones: insights from arc-peridotites. Chem. Geol. 160 (4), 409–423.
Peach, C.L., Mathez, E.A., Keays, R.R., 1990. Sulfide melt-silicate melt distribution coefficients for noble metals and other chalcophile elements as deduced from MORB: implications for partial melting. Geochim. Cosmochim. Acta 54 (12), 3379–3389.
Pearce, J.A., 1982. Trace elements characteristics of lavas from destructive plate boundaries. In: Thorpe, R.S. (Ed.), Andesites: Orogenic Andesites and Related Rocks. Wiley, New York, pp. 525–548.
Pearce, J.A., 1983. The role of sub-continental lithosphere in magma genesis at destructive plate margins. In: Hawkesworth, C.J., Norry, M.J. (Eds.), Continental Basalts and Mantle Xenoliths. Shiva, Nantwich, pp. 230–249.
Pearce, J.A., Peate, D.W., 1995. Tectonic implications of the composition of volcanic arc magmas. Annu. Rev. Earth Planet. Sci. Lett. 23, 251–285.
Peltonen, P., 1995a. Magma–country rock interaction and the genesis of Ni–Cu deposits in the Vammala Nickel Belt, SW Finland. Mineral. Petrol. 52 (1), 1–24.
Peltonen, P., 1995b. Petrogenesis of ultramafic rocks in the Vammala Nickel Belt: implications for crustal evolution of the early Proterozoic Svecofennian arc terrane. Lithos 34 (4), 253–274.
Pettigrew, N., Hattori, K., 2006. The Quetico intrusions of Western Superior Province: Neo-Archean examples of Alaskan/Ural-type mafic–ultramafic intrusions. Precambrian Res. 149 (1), 21–42.
Pirajno, F., 2010. Intracontinental strike-slip faults, associated magmatism, mineral systems and mantle dynamics: examples from NW China and Altay-Sayan (Siberia). J. Geodyn. 50, 325–346.
Pirajno, F., Mao, J.W., Zhang, Z.H., Chai, F.M., 2008. The association of mafic–ultramafic intrusions and A-type magmatism in the Tian Shan and Altay orogens, NW China: implications for geodynamic evolution and potential for the discovery of new ore deposits. J. Asian Earth Sci. 32 (2–4), 165–183.
Plank, T., Langmuir, C.H., 1998. The chemical composition of subducting sediment and its consequences for the crust and mantle. Chem. Geol. 145 (3–4), 325–394.
Qi, L., Hu, J., Gregoire, D.C., 2000. Determination of trace elements in granites by inductively coupled plasma mass spectrometry. Talanta 51 (3), 507–513.
Qian, Z.Z., Sun, T., Tang, Z.L., Jiang, C.Y., He, K., Xia, M.Z., Wang, J.Z., 2009. Platinum-group elements geochemistry and its significances of the Huangshandong Ni–Cu sulfide deposit East Tianshan, China. Geol. Rev. 55, 873–884 (in Chinese with English abstract).
Qin, K.Z., Fang, T.H., Wang, S.L., Zhu, B.Q., Feng, Y.M., Yu, H.F., Xiu, Q.Y., 2002. Plate tectonics division, evolution and metallogenic settings in eastern Tianshan mountains, NW-China. Xinjiang Geol. 20 (4), 302–308 (in Chinese with English abstract).
Qin, K.Z., Zhang, L.C., Xiao, W.J., Xu, X.W., Yan, Z., Mao, J.W., 2003. Overview of major Au, Cu, Ni and Fe deposits and metallogenic evolution of the eastern Tianshan Mountains, Northwestern China. In: Mao, J.W., Goldfarb, R., Seltmann, R., Wang, D.H., Xiao, W.J., Hart, C. (Eds.), Tectonic Evolution and Metallogeny of the Chinese Altay and Tianshan. , 10. IAGOD Guidebook Series, London, pp. 227–248.
Qin, K.Z., Sun, B.X., Sakyi, P.A., Tang, D.M., Li, X.H., Sun, H., Xiao, Q.H., Liu, P.P., 2011. SIMS zircon U–Pb geochronology and Sr–Nd isotopes of Ni–Cu-bearing mafic–ultrafic intrusions in Eastern Tianshan and Beishan in correlation with flood basalts in Tarim basin (NW China): constraints on a ca. 280 Ma mantle plume. Am. J. Sci. 311 (3), 237–260.
Ripley, E.M., 2009. Magmatic Sulfide Mineralization in Alaskan-type Complexes. In: Li, C.S., Ripley, E.M. (Eds.), 7. Geological Publishing House, Beijing, pp. 219–228.
Ripley, E.M., Li, C.S., 2002. Paragneiss assimilation in the genesis of magmatic Ni–Cu–Co sulfide mineralization at Voisey's Bay, Labrador: δ34S, δ13C, and Se/S evidence. Econ. Geol. 97 (6), 1307–1318.
Ripley, E.M., Taib, N., Li, C., Moore, C., 2007. Chemical and mineralogical heterogeneity in the basal zone of the Partridge River Intrusion: implications for the origin of Cu–Ni sulfide mineralization in the Duluth Complex, midcontinent rift system. Contrib. Mineral. Petrol. 154 (1), 35–54.
Roeder, P.L., Emslie, R.F., 1970. Olivine-liquid equilibrium. Contrib. Mineral. Petrol. 29 (4), 275–289.
Rudnick, R., Fountain, D., 1995. Nature and composition of the continental crust: a lower crustal perspective. Rev. Geophys. 33 (3), 267–309.
Ryan, B., 2000. The Nain–Churchill boundary and the Nain Plutonic Suite: A regional perspective on the geologic setting of the Voisey's Bay Ni–Cu–Co deposit. Econ. Geol. 95 (4), 703–724.
San, J.Z., Qin, K.Z., Tang, D.M., Su, B.X., Sun, H., Xiao, Q.H., Liu, P.P., Cao, M.J., 2010. Precise zircon U–Pb ages of Tulargen large Cu–Ni–ore bearing mafic–ultramafic complex and their geological implications. Acta Petrol. Sin. 26 (10), 3027–3035 (in Chinese with English abstract).
Sengör, A.M.C., Natal'in, B.A., Burtman, V.S., 1993. Evolution of the Altaid tectonic collage and Paleozoic crustal growth in Asia. Nature 364, 299–307.
Song, X.Y., Li, X.R., 2009. Geochemistry of the Kalatongke Ni–Cu–(PGE) sulfide deposit, NW China: implications for the formation of magmatic sulfide mineralization in a postcollisional environment. Miner. Deposita 44 (3), 303–327.
Song, B., Li, J.Y., Li, W.Q., Wang, K.Z., Wang, Y., 2002. SHRIMP dating of zircons from Dananhu and Kezirkalasati granitoid batholith in southern margin of Tuha basin and their geological implication. Xinjiang Geol. 20 (4), 342–345 (in Chinese with English abstract).
Song, X.Y., Zhou, M.F., Tao, Y., Xiao, J.F., 2008. Controls on the metal compositions of magmatic sulfide deposits in the Emeishan large igneous province, SW China. Chem. Geol. 253 (1–2), 38–49.
Song, X.Y., Xie, W., Deng, Y.F., Crawford, A.J., Zheng, W.Q., Zhou, G.F., Deng, G., Chen, S.L., Li, J., 2011a. Slab break-off and the formation of Permian mafic–ultramafic intrusions in southern margin of Central Asian Orogenic Belt, Xinjiang, NW China. Lithos 127 (1–2), 128–143.
Song, X.Y., Wang, Y.S., Chen, L.M., 2011b. Magmatic Ni–Cu–(PGE) deposits in magma plumbing systems: features, formation and exploration. Geosci. Front. 2 (3), 375–384.
Stein, R., 1990. Organic carbon content/sedimentation rate relationship and its paleoenvironmental significance for marine sediments. Geo-Mar. Lett. 10, 37–44.
Su, B.X., Qin, K.Z., Sakyi, P.A., Li, X.H., Yang, Y.H., Sun, H., Tang, D.M., Liu, P.P., Xiao, Q.H., Malaviarachchi, S.P., 2011. U–Pb ages and Hf–O isotopes of zircons from Late Paleozoic mafic–ultramafic units in the southern Central Asian Orogenic Belt: tectonic implications and evidence for an Early-Permian mantle plume. Gondwana Res. 20 (2–3), 516–531.
Su, B.X., Qin, K.Z., Su, H., Tang, D.M., Sakyi, P.A., Chu, Z.Y., Liu, P.P., Xiao, Q.H., 2012. Subduction-induced mantle heterogeneity beneath Eastern Tianshan and Beishan: insights from Nd–Sr–Hf–O isotopic mapping of Late Paleozoic mafic–ultramafic complexes. Lithos 134–135, 41–51.
Sun, S.S., McDonough, W., 1989. Chemical and isotopic systematics of oceanic basalts: implications for mantle composition and processes. Geol. Soc. Lond. Spec. Publ. 42 (1), 313–345.
Sun, H., Qin, K.Z., Li, J.X., Xu, X.W., San, J.Z., Ding, K.S., Hui, W.D., 2006. Petrographic and geochemical characteristics of the Tulargen Cu–Ni–Co sulfide deposit, East Tianshan, Xinjiang, and its tectonic setting. Geol. China 33 (3), 606–617.
Tang, D.M., Qin, K.Z., Li, C.S., Qi, L., Su, B.X., Qu, W.J., 2011. Zircon dating, Hf–Sr–Nd–Os isotopes and PGE geochemistry of the Tianyu sulfide-bearing mafic–ultramafic intrusion in the Central Asian Orogenic Belt, NW China. Lithos 126, 84–98.
Tang, D.M., Qin, K.Z., Sun, H., Su, B.X., Xiao, Q.H., 2012. The role of crustal contamination in the formation of Ni–Cu sulfide deposits in Eastern Tianshan, Xinjiang, Northwest China: evidence from trace element geochemistry, Re–Os, Sr–Nd, zircon Hf–O, and sulfur isotopes. J. Asian Eart Sci. 49, 145–160.
Taylor, J.H., 1967. The zoned ultramafic complexes of southeastern Alaska. In: Wyllie, P.J. (Ed.), Ultramafic and Related Rocks. John Wiley and Sons Incorporated, New York, pp. 97–121.
Thakurta, J., Ripley, E.M., Li, C.S., 2008. Geochemical constraints on the origin of sulfide mineralization in the Duke Island Complex, southeastern Alaska. Geochem. Geophys. Geosyst. 9 (7), Q07003.
Theriault, R.D., Barnes, S.J., 1998. Compositional variations in Cu–Ni–PGE sulfides of the Dunka Road deposit, Duluth Complex, Minnesota: the importance of combined assimilation and magmatic processes. Can. Mineral. 36 (3), 869–886.
Tomkins, A.G., Rebryna, K.C., Weinberg, R.F., Schaefer, B.F., 2012. Magmatic sulfide formation by reduction of oxidized arc basalt. J. Petrol. 53 (8), 1537–1567.
Tornos, F., Casquet, C., Galindo, C., Velasco, F., Canales, A., 2001. A new style of Ni–Cu mineralization related to magmatic breccia pipes in a transpressional magmatic arc, Aguablanca, Spain. Miner. Deposita 36 (7), 700–706.
Tornos, F., Galindo, C., Casquet, L., Rodríguez, P.C., Martínez, E., Martínez, F., Velasco, A., Iriondo, A., 2006. The Aguablanca Ni–(Cu) sulfide deposit, SW Spain: geologic and geochemical controls and the relationship with a midcrustal layered mafic complex. Miner. Deposita 41 (8), 737–769.

Wang, R.M., Liu, D.Q., Ying, D.T., et al., 1987. Cu–Ni sulfide deposits in the Tudun–Huangshan region, Hami, Xinjiang: Genet controls exploration implications. Miner Rocks 7, 1–152 (in Chinese).
Wang, K.L., Chung, S.L., Reilly, S.Y., Sun, S.S., Shinjo, R., Chen, C.H., 2004a. Geochemical constraints for the genesis of post–collisional magmatism and the geodynamic evolution of the Northern Taiwan Region. J. Petrol. 45 (5), 975–1011.
Wang, Y.W., Wang, J.B., Wang, L.J., Fang, T.H., 2004b. REE characteristics of Cu–Ni sulfide deposits in the Hami area, Xinjiang. Acta Petrol. Sin. 20 (4), 935–948 (in Chinese with English abstract).
Wartes, M.A., Carroll, A.R., 2002. Permian sedimentary record of the Turpan–Hami basin and adjacent regions, northwest China: constraints on postamalgamation tectonic evolution. Geol. Soc. Am. 114 (2), 131–152.
Wilson, M., 1989. Igneous Petrogenesis. Unwin Hyman, London 1–466.
Windley, B.F., Alexeiev, D., Xiao, W.J., Kröner, A., Badarch, G., 2007. Tectonic models for accretion of the Central Asian Orogenic Belt. J. Geol. Soc. Lond. 164, 31–47.
Wu, F.Y., Wilde, S.A., Zhang, G.L., Sun, D.Y., 2004. Geochronology and petrogenesis of the post-orogenic Cu–Ni sulfide-bearing mafic–ultramafic complexes in Jilin Province, NE China. J. Asian Earth Sci. 23, 781–797.
Wyllie, P.J., 1982. Subduction products according to exprimental prediction. Bull. Geol. Soc. Am. 93 (6), 468–476.
Xiao, W.J., Zhang, L.C., Qin, K.Z., Sun, S., Li, J.L., 2004. Paleozoic accretionary and collisional tectonics of the Eastern Tianshan (China): implications for the continental growth of central Asia. Am. J. Sci. 304, 370–395.
Xiao, W.J., Han, C.M., Yuan, C., Sun, M., Lin, S.F., Chen, H.L., Li, Z.L., Li, J.L., Sun, S., 2008. Middle Cambrian to Permian subduction-related accretionary orogenesis of Northern Xinjiang, NW China: implications for the tectonic evolution of central Asia. J. Asian Earth Sci. 32 (2–4), 102–117.
Xiao, W.J., Mao, Q.G., Windley, B.F., Han, C.M., Qu, J.F., Zhang, J.E., Ao, S.J., Guo, Q.Q., Ckeven, N.R., Lin, S.F., Shan, Y.H., Li, J.L., 2010. Paleozoic multiple accretionary and collisional processes of the Beishan Orogenic Collage. Am. J. Sci. 310, 1553–1594.
Yang, S.H., Zhou, M.F., Lightfoot, P.C., Malpas, J., Qu, W.J., Zhou, J.B., Kong, D.Y., 2012. Selective crustal contamination and decoupling of lithophile and chalcophile element isotopes in sulfide-bearing mafic intrusions: an example from the Jingbulake intrusion, Xinjiang, NW China. Chem. Geol. 302–303 (2), 106–118.
Yuan, C., Sun, M., Wilde, S., Xiao, W.J., Xu, Y.G., Long, X.P., Zhao, G.C., 2010. Post-collisional plutons in the Balikun area, East Chinese Tianshan: evolving magmatism in response to extension and slab break-off. Lithos 119 (3–4), 269–288.
Zhang, Z.C., Yan, S.H., Chen, B.L., He, L.X., He, Y.S., Zhou, G., 2003. Geochemistry of the Kalatongke basic complex in Xinjiang and its constraints on genesis of the deposit. Acta Petrol. Mineral. 22 (3), 217–224 (in Chinese with English abstract).
Zhang, L.C., Qin, K.Z., Ying, J.F., Xia, B., Shu, J.S., 2004. The relationship between oreforming processes and adakitic rock in Tuwu-Yandong porphyry copper metallogenic belt, eastern Tianshan mountains. Acta Petrol. Sin. 20 (2), 259–268 (in Chinese with English abstract).
Zhang, Z.C., Yan, S.H., Chen, B.L., He, L.X., He, Y.S., Zhou, G., Chai, F.M., 2006. Sr, Nd and O isotope geochemistry of the mafic–ultramafic complexes in the south margin of Altay orogenic belt and discussion on their sources. Geol. Rev. 52 (1), 38–42 (in Chinese with English abstract).
Zhang, C., Li, X., Li, Z., Ye, H., Li, C., 2008. A Permian layered intrusive complex in the western Tarim Block, northwestern China: Product of a ca. 275-Ma mantle plume? J. Geol. 116 (3), 269–287.
Zhang, Z.C., Mao, J.W., Chai, F.M., Yan, S.H., Chen, B.L., Pirajno, F., 2009. Geochemistry of the Permian Kalatongke mafic intrusions, Northern Xinjiang, Northwest China: implications for the genesis of magmatic Ni–Cu sulfide deposits. Econ. Geol. 104 (2), 185–203.
Zhang, M.J., Li, C.S., Fu, P.E., Hu, P.Q., Ripley, E.M., 2011. The Permian Huangshanxi Cu–Ni deposit in western China: intrusive–extrusive association, ore genesis, and exploration implications. Miner. Deposita 46 (2), 153–170.
Zhou, M.F., Lesher, C.M., Yang, Z.X., Li, J.W., Sun, M., 2004. Geochemistry and petrogenesis of 270 Ma Ni–Cu–(PGE) sulfide-bearing mafic intrusions in the Huangshan District, eastern Xinjiang, northwest China; implications for the tectonic evolution of the Central Asian orogenic belt. Chem. Geol. 209 (3–4), 233–257.
Zhou, D.W., Liu, Y., Xing, X.J., Hao, J.R., Dong, Y.P., Ouyang, Z.J., 2006. Formation of the Permian basalts and imply.ations of geochemical tracing for paleo-tectonic setting and regional tectonic background in the Turpan–Hami and Santanghu basins, Xinjiang. Sci. China Ser. D 49 (6), 584–596.
Zhou, M.F., Zhao, J.H., Jiang, C.Y., Gao, J.F., Wang, W., Yang, S.H., 2009. OIB-like, heterogeneous mantle sources of Permian basaltic magmatism in the western Tarim Basin, NW China: implications for a possible Permian large igneous province. Lithos 113, 583–594.
Zhou, T.F., Yuan, F., Zhang, D.Y., Fan, Y., Liu, S., Peng, M.X., Zhang, J.D., 2010. Geochronology, tectonic setting and mineralization of granitoids in Jueluotage area, eastern Tianshan, Xinjiang. Acta Petrol. Sin. 26 (2), 478–502 (in Chinese with English abstract).